Catalysis Letters (2021) 151:3417–3436
https://doi.org/10.1007/s10562-021-03576-x

PERSPECTIVE

On the Role and Applications of Electron Magnetic Resonance Techniques in Surface Chemistry and Heterogeneous Catalysis

Mario Chiesa[1] · **Elio Giamello**[1]

Received: 3 February 2021 / Accepted: 17 February 2021 / Published online: 16 March 2021

Abstract

Some relevant aspects of Electron Paramagnetic Resonance (EPR) applied to the fields of surface chemistry and heterogeneous catalysis are illustrated in this perspective paper that aims to show the potential of these techniques in describing critical features of surface structures and reactivity. Selected examples are employed covering distinct aspects of catalytic science from morphological analysis of surfaces to detailed descriptions of chemical bonding and catalytic sites topology. In conclusions the pros and cons related to the acquisition of EPR instrumentations in an advanced laboratory of surface chemistry and heterogeneous catalysis are briefly considered.

Graphic Abstract

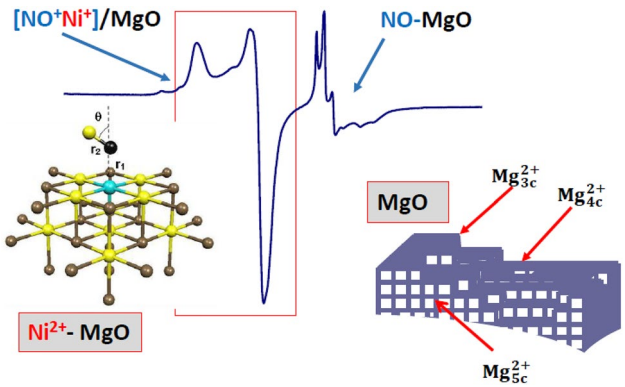

Keywords Electron magnetic resonance · Heterogeneous catalysis · Surface chemistry · Catalysis, oxide supports · Zeolites · Ziegler–Natta

1 Introduction

Electron Paramagnetic Resonance, EPR, has been employed in experimental research on surface chemistry and heterogeneous catalysis since the beginning of the sixties. This technique, after the first experiment performed by E. Zavoisky's in USSR in 1944, was independently developed in the same period in Oxford by B. Bleaney and a group of theoretical physicists (Abragam, Pryce) who laid the foundations of the discipline. The first applications of the EPR technique were devoted to the properties of transition metal ions compounds and those of paramagnetic defects in the solid state. The important achievements in these two research areas combined with the sensitivity of the technique and the unique level of detail in the description of those features of

✉ Elio Giamello
elio.giamello@unito.it

Mario Chiesa
mario.chiesa@unito.it

[1] Dipartimento di Chimica, Università degli Studi di Torino, Via P. Giuria 7, 10125 Turin, Italy

the electron wave function related to the unpaired electron distribution, stimulated the application of the technique to the study of surface chemistry and heterogeneous catalysts.

The first review article concerning applications of EPR to heterogeneous catalysis dates back to 1960 [1] and is relatively poor of experimental data. Much more results are found in review papers intermittently appeared later [2–11] and describing the growing role of EPR in characterizing systems of interest for heterogeneous catalysis such as adsorbed paramagnetic molecules, surface defects centres, surface reaction intermediates and supported transition metal ions. Recently, beside the classic EPR acronym, the broader Electron Magnetic Resonance (EMR) one has been introduced that includes a variety of experimental approaches involving the interactions of electron magnetic dipoles with an external magnetic field. Both acronyms will be used in the present article that has been written with the aim of answering two elementary questions. The former one is: what are the main aspects of surface chemistry and heterogeneous catalysis that can conveniently be investigated by electron magnetic resonance techniques? The second one is: what are the potential advantages (and the disadvantages) for a research group in these disciplines that intends to invest in an EPR instrumentation? The answer to the former question will be provided using a number of specific examples mainly derived from the experience of our group and covering distinct areas the catalytic sciences.

The paper is organized as follows. In the first part, the principles of the EPR technique will be concisely described, referring to specific contributions available in the literature for more in-depth treatments. In the central part, some topics of surface chemistry and catalysis will be illustrated through specific examples showing the capability of EPR to play an important role in the advancement of knowledge. In conclusion, the advantages of EMR and the disadvantages, that inevitably limit an even more widespread use of these techniques, will be briefly discussed.

2 Basic Features of Electron Magnetic Resonace

The conventional continuous wave (CW) EPR is, among the various EMR techniques, the dominant one in heterogeneous catalysis studies. The distinctive feature of EPR is that it exclusively monitors paramagnetic species i.e. chemical entities bearing one or more unpaired electrons and is blind to all diamagnetic entities. This is a clear disadvantage in view of a broad application of the technique but this selectivity can also be thought as an advantage, considering that a given paramagnetic center belonging to a complex chemical system (e.g. a paramagnetic ion in a protein or dispersed in a zeolitic framework) can be studied without any interference. Clearly, care must be taken to make sure that the active paramagnetic species is also a catalytically relevant species. To be complete it has also to be taken in mind that, in some particular instances, there are paramagnetic species escaping EPR detection, because of mutual physical interactions due to their close proximity.

Electron magnetic resonance occurs when an electromagnetic wave of suitable frequency (usually in the microwave region) interacts with the sample immersed in an applied magnetic field and causes the inversion of the spin (and thus of the magnetic moment) of the unpaired electrons so that a certain amount of electromagnetic energy is absorbed by the system. Considering a free electron, the effect of an applied magnetic field $\boldsymbol{B}$ is to generate two distinct spin states (Zeeman effect). The electrons in the lower state (β) can be promoted in the upper state (α) by absorption of a quantum of electromagnetic radiation energy, $h\nu$, coinciding with the energy difference between the two states

$$h\nu = g\ \mu_B B \tag{1}$$

where ν is the radiation frequency, $g = 2.0023$ the free electron g value and μ_B a constant called the Bohr magneton. The EPR spectra are usually reported, for technical reasons, as the first derivative of the microwave absorption as a function of the swept magnetic field. The most commonly used microwave frequency in the study of heterogeneous catalysts and photocatalysts is ca. 9.5 GHz in the range of the so called X-band, 8–12 GHz, the most often used in radar applications. In this case the magnetic induction necessary to observe the resonance of a free electron or of a simple organic radical falls around 350 mT. Other regions of microwave frequencies used in commercial EPR spectrometers are Q-band (around 35 GHz) and W-band (95 GHz). Continuous wave techniques include CW-EPR, ENDOR (Electron Nuclear Double Resonance) and HF-EPR (High Field EPR).

Similarly to what was done in Nuclear Magnetic Resonance, pulsed methods were also introduced in EPR, though more recently. The reason why the development of commercial pulse EPR spectrometers lagged behind that of NMR is related to the much faster electron relaxation times, which are of the order of 10^6 times faster than those of nuclei, requiring pulse timimings $\approx 10^6$ times shorter for pulsed EPR than for pulsed NMR. This fact not only slowed down the evolution of commercial pulse EPR spectrometers with respect to NMR but poses some limit to the application of pulse EPR techniques especially in catalytic systems featuring the presence of nanoparticles or high spin states. On the other hand, when applicable, the selectivity and resolution of pulse EPR experiments, in particular of so called hyperfine techniques of ENDOR and ESEEM (Electron Spin Echo Envelope Modulation), can provide sub-MHz resolution,

allowing to couple the sensitivity and selectivity of EPR with the resolution of NMR. Under such circumstances coordination spheres up to the third can be investigated.

The EPR spectrum of a paramagnetic species is the result of a series of interactions of the unpaired electron(s) with the surroundings and it can be described in terms of a spin Hamiltonian, that is a series of energy terms each one corresponding to a distinct interaction. For the purposes of the present paper it is sufficient to consider the following three terms of the spin-Hamiltonian.

$$\mathcal{H} = \mu_B \boldsymbol{S} \cdot \boldsymbol{g} \cdot \boldsymbol{B} + \boldsymbol{S} \cdot \boldsymbol{A} \cdot \boldsymbol{I} + \boldsymbol{S} \cdot \boldsymbol{D} \cdot \boldsymbol{S} \quad (2)$$

The first term (electronic Zeeman operator) accounts for the interaction of the electron spin $\boldsymbol{S}$ with the external magnetic field $\boldsymbol{B}$. The interaction is determined by the $\boldsymbol{g}$ tensor, a 3×3 matrix which, in general, can be reduced to its diagonal form. The tensorial nature of g indicates that the resonant magnetic field varies according to the orientation of the paramagnetic species in the magnetic field itself. The values of the diagonal elements of the $\boldsymbol{g}$ tensor (that are somehow equivalent to the chemical shift in NMR) depend on the electronic structure (ground and excited states) of the paramagnetic species.

The second term represents the interaction between electron spin and nuclear spins (hyperfine interaction, hpf). $\boldsymbol{A}$ is the hyperfine tensor and $\boldsymbol{I}$ is the nuclear spin vector. In CW-EPR the hyperfine interaction gives rise to the so called hyperfine structure. A set of $2I+1$ lines is expected (for any given orientation of the species into the magnetic field) for the interaction of the electron spin with a nucleus having non-zero nuclear spin (quantum number $I \neq 0$). $\boldsymbol{A}$ is composed of two main contributions, i.e. the isotropic Fermi contact term a_{iso} (a scalar related to electron spin density in the volume of the nucleus observed for s-type orbitals only) and the anisotropic electron-nucleus dipolar coupling expressed by a matrix $\boldsymbol{T}$. The term hyperfine interaction is typically associated to the interaction between the unpaired electron of a given species and the nuclei belonging to the species itself. The same type of interaction, when it involves magnetic nuclei of entities surrounding the magnetic centre (such as the ligands in the case of a coordination compound) is sometimes referred to as super-hyperfine (*shf*) interaction.

The third term describes the interaction between two or more unpaired electrons ($S > 1/2$) which is gauged by the $\boldsymbol{D}$ tensor. Systems with $S > 1/2$ are frequent in the case of transition metal ions. Ions such as Fe^{3+} or Mn^{2+} in high spin configuration, for instance, are characterized by $S = 5/2$. The **D** tensor can be expressed in terms of two quantities (D and E) that account for the "zero-field splitting", the interaction between unpaired electrons occurring in the absence of the external magnetic field.

The tensors present in all terms of Eq. 1 reflect the anisotropy of magnetic interactions. This means that, when the paramagnetic system is located in a single crystal, the EPR signal changes according to the orientation of the crystal in the external magnetic field $\boldsymbol{B}$. A careful measure of all the magnetic tensor components is obtained, in this case, recording the EPR spectrum at various orientations of the crystal axes in the applied magnetic field.

Single crystals have been employed in EPR studies of surface science and catalysis in few cases only. Much more common, in particular in the case of real heterogeneous catalysts, are disordered systems e.g. polycrystalline materials (or powders) composed by many crystallites casually oriented in space. In this case the shape of the "powder spectrum" does not vary with the orientation of the sample in the external field and contains, in principle, all the information about the magnetic tensors in Eq. 1. The EPR powder spectrum is the envelope of single spectra corresponding to all possible orientations of the paramagnetic species with respect to the applied magnetic field. The presence of resonance in a range of magnetic field (say, B_{min}–B_{max}) does not create, however, a uniform envelope. The microwave absorption reported as a function of the resonant field B_{res} has turning points for orientations corresponding to the principal (or diagonal) components of the g tensor which show up in the first derivative spectral trace. Figure 1 shows three examples of powder spectra. In the first two cases there is no hyperfine interaction ($I = 0$) and the information is limited to the only g tensor which is axial in the first case (Fig. 1a, $g_{zz} = g_{\parallel}$, $g_{xx} = g_{yy} = g_{\perp}$) and rhombic in the second one (Fig. 1b, $g_{zz} \neq g_{xx} \neq g_{yy}$ or, when the directions of g axes are unknown, $g_1 \neq g_2 \neq g_3$). In Fig. 1c the g tensor in the same of Fig. 1b but

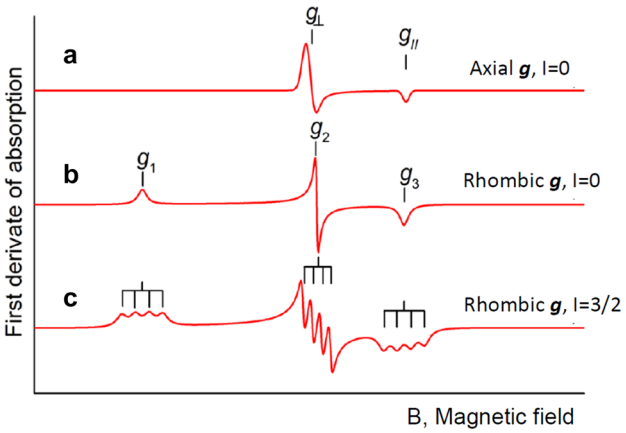

Fig. 1 Calculated spectral profiles of the EPR powder spectra (first derivative of absorption as a function of the swept magnetic field) in the case of an axial g tensor (a) and a rhombic g tensor in the absence of hyperfine interactions (b). The profile in (c) is based on the g tensor of the species in (b) with the onset of a hyperfine interaction with a nucleus having I = 3/2 (four lines)

the three principal components are split in four lines due to hyperfine interaction with a nucleus having I = 3/2.

It should be outlined that all cases in Fig. 1 report a signal related to a single paramagnetic species containing information on the three principal values of the g tensor. It is thus mistaken to treat (as unfortunately it can be found in some examples present in the literature) the various g components as independent features corresponding to distinct species.

Determining the exact *g* and *A* values in real cases can be difficult. This is due to several factors such as: (i) the presence of more than one species with overlapping signals (the range of the observed *g* values is relatively limited for a large fraction of the more common paramagnetic species), (ii) poor resolution of the hyperfine structure, (iii) line broadening due to magnetic interactions between nearby species. For this reason it is often necessary, for an unambiguous assignment of the spectra, the use of tools such as multifrequency EPR (recording spectra at more than one frequency) and isotopic substitution (inserting atoms with different nuclear spin in the paramagnetic species or in its surroundings). Furthermore, the computer simulation of the experimental spectra is an essential good practice to verify and to refine the set of spin-Hamiltonian parameters derived from a preliminary analysis of the spectrum and, in the recurrent case of the simultaneous presence of various paramagnetic species, to evaluate the abundance of each of them.

Among the above mentioned pulse-EPR techniques, particular emphasis, in this paper, will be given to HYSCORE (Hyperfine Sublevel Correlation spectroscopy). This is a two dimensional technique based on a particular pulse sequence that creates a correlation between the nuclear frequencies in the two spin manifolds allowing the observation of NMR transitions related to nuclei in the surroundings of the paramagnetic centre. An HYSCORE experiment, similarly to the ENDOR experiment, is particularly appropriate to measure weak hyperfine interactions undetectable by CW-EPR, which can however be very revealing of the coordination environment and catalytic function of paramagnetic species. A review on the advantages of high field ENDOR in the characterization of functional sites in microporous materials can be found in ref. [12], while some case studies are reported in ref [13–16]. Several comprehensive textbooks are available for the reader interested to a deeper knowledge of the physical bases of electron magnetic resonance and of the mentioned advanced techniques [17–22].

3 EPR in Surface Chemistry and Catalysis

A classic CW-EPR spectrometer is built up to allow the interaction of microwaves having a fixed frequency with a sample kept into the lines of force of a variable magnetic field. In short, the technical apparatus is based on a microwave bridge that generates microwaves which are sent through a wave-guide to a resonant cavity containing the sample and capable to store the microwave energy. The cavity is placed into a homogeneous magnetic field produced by an electromagnet. Despite the size and weight of this experimental apparatus the EPR technique can be adapted to the complex experiments required in catalytic research. The experiments, in fact, can be run in a wide range of temperature. The very low values of liquefied helium (from about 4 K onwards) or nitrogen (from 77 K) are employed to obtain resolved, low-linewidth spectra while the high temperatures typical of real catalytic processes are used in the so called EPR in-operando (see below). The resonant cavity also contains a window that allows the illumination of the sample with light in the range between UV and IR. This allows unique opportunities in the field of photocatalysis e.g. monitoring the excited states of the photocatalyst or following the state of the system during the photocatalytic reaction [23]. Another point in favor of the use of EPR in surface science and catalysis is the high sensitivity of the technique (the limit of detection corresponds to about 10^{12} spin) that allows monitoring low concentration intermediates typical of catalytic phenomena often undetectable by other techniques.

The main experimental issues potentially covered by EPR experiments in surface chemistry and catalysis can be summarized as follows:

- probing the morphological features of surface sites
- nature and properties of reactive surface intermediates
- unravelling the chemical bonding at solid surfaces
- topological description of active sites in catalytic systems
- geometrical and electronic structure of catalytic sites via selective isotopic enrichment
- catalytic sites under real conditions (*operando* EPR)

Specific examples on each item will be illustrated in the following of this paper except for the last one. The reader is referred, in this case, to exhaustive specific reports about EPR in operando that have been published along the years and illustrate in detail the particular feature of such an approach [10, 24–26]. Furthermore, the particular subject of EPR investigation in photocatalysis is mentioned in a Sect. 3.2.2. however not treated in great detail. A specific article on this topic has been recently published [27].

3.1 Probing the Morphological Features of Surface Sites of Metal Oxides

In the Introduction, emphasis was put on the role of EPR in unravelling the features of paramagnetic systems. Actually a second, alternative approach in EPR research exists that is exploring the features of a diamagnetic system

using a paramagnetic molecule acting as spin probe. This approach has been widely used in the investigation of soft matter (membranes, micelles etc.) and it can be also applied to solid surfaces, in particular of metal oxides, in order to monitor the surface crystal fields and for surface sites identification. The most common spin probes employed in the surface chemistry of metal oxides are the superoxide radical ion ($O_2^{\cdot-}$) which has to be generated in some way by a surface reaction or nitric oxide (NO) which, as opposite, can be directly adsorbed on a bare surface.

NO is an 11-electron molecule with one electron in 2π degenerate antibonding orbitals and $^2\Pi_{1/2}$ ground state. The ability of this molecule as a surface probe is twofold in that it can reveal both the surface crystal field of cationic sites and the presence of highly basic O^{2-} oxide ions.

In the former case NO acts as a probe when physisorbed at low temperature [28]. In such conditions the electric field present at the surface of the ionic crystal in correspondence of specific cationic sites splits the energies of the 2π antibonding orbitals by a factor Δ. The EPR spectrum of nitric oxide is based on an orthorhombic g tensor whose g_{zz} component (z is the direction corresponding to the molecular axis) directly depends on Δ according to the following, first-order approximated, equation

$$g_{zz} = g_e - 2\lambda/\Delta \tag{3}$$

The g_{zz} component thus becomes a measure of the electric field felt by the adsorbed nitric oxide (NO).

The EPR spectrum of nitric oxide physisorbed on polycrystalline MgO is reported in Fig. 2.

MgO is a highly ionic basic oxide exhibiting the simple structure of sodium chloride. The coordination 6 of bulk ions reduces to 5, 4 or 3 when the ions are exposed at the surface. Due to its relatively simple features MgO has served has as a model system for the investigations of both surface science [29] and surface chemistry [30] of metal oxides. By the way, a quite spectacular example of the the success of EPR in providing atomistic information of the structure of reactive sites at surfaces indeed concerns this oxide. This is the case of the so-called F_s^+(H) that for a long time were described in terms of oxygen vacancies containing unpaired electrons. However, thanks to high resolution EPR experiments coupled with DFT calculations it was shown that they consist of electrons trapped at particular cationic sites where they are stabilized by the joint action of surface cations and nearby hydroxyl groups [31, 32]. This topic has been the object of specific review papers [33] and will not be further discussed here.

Going back to nitric oxide interaction with MgO, the main features of the EPR spectrum of physisorbed NO is a N hyperfine triplet centered at about $g = 1.99$ (^{14}N is the most abundant—99.6%—nitrogen isotope and has nuclear spin $I = 1$). The spectrum also exhibits, at higher field, three different g_{zz} lines ($g_{zz} = 1.9610$, $g_{zz} = 1.9188$, $g_{zz} = 1.8900$) which are independent one from the other [34]. Each of these high field lines is also split in three components by N hyperfine interaction but the splitting is fully appreciable on the third line only ($g_{zz} = 1.8900$). The spectrum in Fig. 2 (top) has been therefore interpreted in terms of the presence of three NO molecular species weakly adsorbed on three distinct Mg^{2+} sites. The adsorbed NO species differ essentially in the higher field g_{zz}

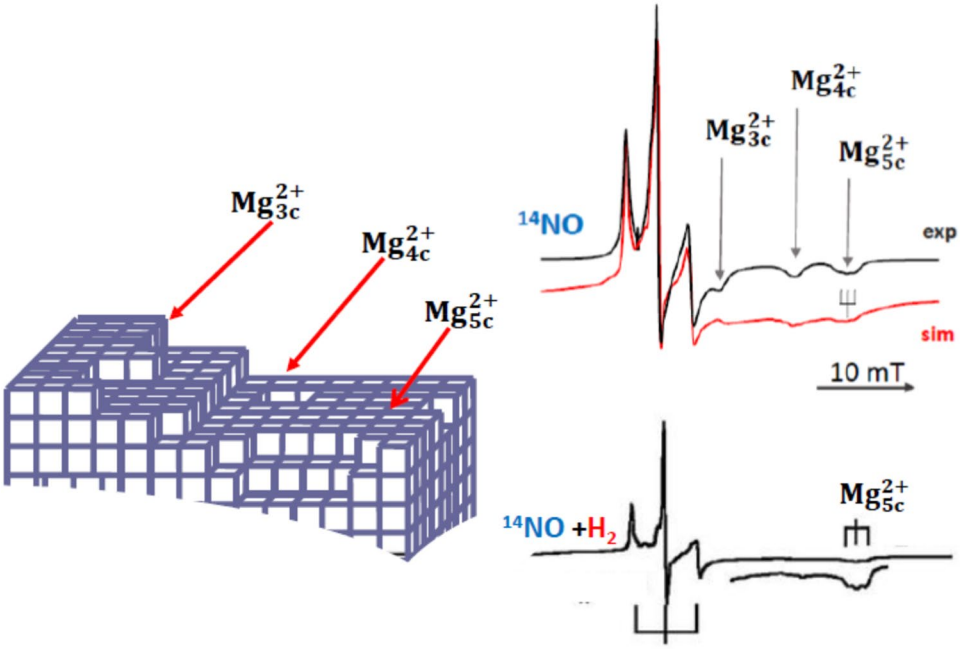

Fig. 2 EPR spectra recorded at 77 K of NO adsorbed on polycrystalline MgO (top, experimental and simulated lines) and of a H_2-NO mixture (10:1) adsorbed on the same surface. In the left hand side, a schematic view of the MgO surface

component (Δ splitting value) reflecting the different polarizing power, hence the Madelung potential of the surface sites. The lower g_{zz}, the higher Δ (Eq. 3). The three surface sites monitored by NO have respectively coordination 5, 4 and 3 (scheme in Fig. 2) as also confirmed by theoretical modelling [34].

Nitric oxide, as a paramagnetic probe, can also be employed to identify the sites responsible of particular surface reactivity. This is the case, for instance, of the heterolytic dissociation of H_2 at the surface of MgO that is fully reversible at room temperature and has been widely investigated in the past. The EPR spectrum in Fig. 2 (bottom) has been recorded after the adsorption of a H_2–NO mixture. It is easy to see that this second spectrum, again due to adsorbed NO, shows the finger print of the 5-coordinated ions only ($g_{zz}=1.89$) firmly indicating that the two other families of low coordination sites (4-c and 3-c) are those involved in the dissociative chemisorption of the hydrogen molecule. The latter process selectively block the lower coordination sites that are no more available for the weak NO polarization [35].

NO is indeed a multitasking probe. In the case of basic oxides it can also probe highly basic O^{2-} ions forming covalently bound NO_2^{2-} adducts which are paramagnetic and have a typical EPR spectrum which can be observed at room temperature in the absence of physisorbed NO. These highly basic sites are a very minor fraction of surface MgO oxide ions but their amount increases moving to oxides with higher basicity such as CaO [36].

The NO molecule is also sensitive to the presence of transition metal ions at the surface due to their propensity to form nitrosyl adducts. An example is that of the interaction with a MgO matrix containing 1% of Ni^{2+} homogeneously dispersed in the solid matrix (MgO and NiO have the same NaCl structure and are soluble in the whole range of concentrations). Probing the surface of this solid solutions by NO adsorption, the spectrum in Fig. 3 shows up. Remarkably NO is still capable to monitor the Mg^{2+} surface sites (the signal at high field in Fig. 2 is the same discussed above) even though the spectrum is dominated by an intense axial signal at lower field. This has the structure with $g_{\parallel} > g_{\perp} > g_e$ typical of the spectrum of $3d^9$ ions and is due to Ni^+ ions that forms by interaction of NO with Ni^{2+} ions at the MgO terrace.

Such an interaction is essentially an electron transfer from the molecule to the surface ion that leads to the formation of an adduct schematically indicated as Ni^+NO^+ [37]. Theoretical calculations confirm this picture describing in detail the nature of this bent nitrosylic adduct (see Scheme in Fig. 3) which host the unpaired electron in the Ni d_{x2-y2} orbital.

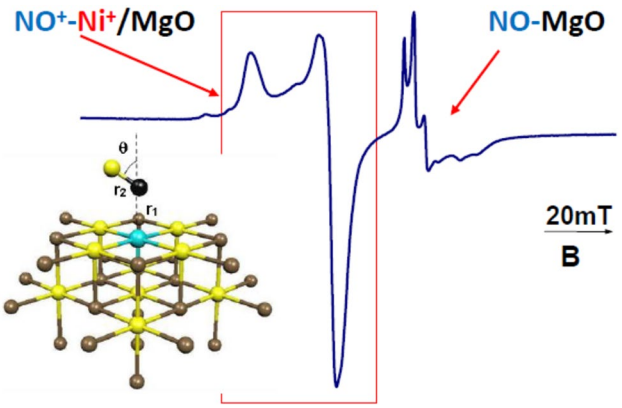

Fig. 3 EPR spectrum obtained by NO adsorption on the surface of a Ni–MgO solid solution (1 mol%). The scheme shows the structure of the bent nitrosyl adduct on Ni ions

3.2 Nature and Properties of Reactive Surface Intermediates

3.2.1 Superoxide Intermediates in Oxidation of Alkenes on MgO and C–H Heterolytic Splitting

Catalytic materials based on metal oxides have a dominant role in heterogeneous catalysis and, in parallel, molecular oxygen is an important reactant in several catalytic processes. It is therefore understandable that oxygen species at the surface of oxides play a crucial role in many heterogeneous processes. The classic Mars–Van Krevelen mechanism for selective oxidation of hydrocarbons, for instance, epitomizes this concept since it involves the incorporation of gas phase oxygen into the bulk of the oxide catalyst that loses oxygen while oxidizing the organic substrate. Oxygen incorporation is thought to occur via a stepwise reduction involving the formation of various reactive intermediates some of which are paramagnetic

$$O_{2(g)} \rightarrow O^{\cdot-}_{2\,ads} \rightarrow O^{2-}_{2\,ads} \rightarrow O^{\cdot-}_{ads} \rightarrow O^{2-}_{surf} \quad (4)$$

All species present in Eq. 4 are highly reactive and can be formed not only by reduction of molecular oxygen but also via different processes occurring at the surface. Two of them ($O_2^{\cdot-}$ and $O^{\cdot-}$) are paramagnetic and may be monitored by EPR. We will refrain here to report details on the structure of the EPR spectra of these two species that are widely discussed elsewhere [38, 39], limiting ourselves to

shortly illustrate two examples with oxygen reactive species playing a key role in complex reaction mechanisms. As it will be shown the detection by EPR of these paramagnetic intermediates contributes to elucidate details of the mechanism itself.

The oxidation of alkenes in mild conditions on the surface of magnesium oxide was described years ago. In the case of propene, the reaction is initiated by the basic action of the surface O^{2-} ions. These are able to heterolytically split the C–H bond abstracting a proton and forming the corresponding carbanion [40]

$$C_3H_5{-}H + O^{2-}_{surf} \rightarrow C_3H^-_{5\,(ads)} + OH^-_{surf} \tag{5}$$

The surface adsorbed carbanion is unstable and in presence of oxygen an electron transfer occurs producing surface adsorbed superoxide ions (which can be monitored by EPR) and a reactive organic radical:

$$C_3H^-_{5\,(ads)} + O_{2(g)} \rightarrow \cdot C_3H_5 + O^{\cdot-}_{2\,(ads)} \tag{6}$$

This mechanism, indicated as surface intermolecular electron transfer (SIET) [41] continues with formation of oxygenated compounds such as acetates, formates and carbonates. The kinetics is zero order with respect to propene and second order with respect to the adsorbed O_2^- intermediate with a typical Langmuir–Hinselwood mechanism [42]. The direct observation of adsorbed superoxide ions upon co-adsorption of a hydrocarbon and oxygen is therefore diagnostic of the presence of a basic sites capable of heterolytic splitting of C–H bonds having extremely low acidity (Eq. 5). Propene (pKa = 35) is split at the surface of MgO while methane (pKa = 40) is not. This ability typical of basic oxide ions increases moving from MgO to the other alkali-earth oxides. In the case of calcium oxide, the formation of superoxide has been observed for saturated hydrocarbons with acidity lower than that of propene (pKa ≅ 40).

Figure 4 reports the energy levels of an adsorbed superoxide. This is a 13e-π radical whose π antibonding degenerate orbitals are split by a factor Δ by the crystal field of the adsorbing cation. In analogy to what described for the NO molecule (Sect. 3.1) the z component of the g tensor (z is the O–O axis direction) is sensitive to this splitting being

$$g_{zz} = g_e + 2\lambda/\Delta \tag{7}$$

Notice that the formula is similar to that in Eq. (3), the inversion of the sign being due to the difference between the NO configuration (one electron in the 2π* orbitals) and that of O_2^- (one hole in the same orbitals). A schematic EPR signal of adsorbed superoxide is also shown in Fig. 4 top. The signal is rhombic with the g_{yy} and g_{xx} components quite close one to the other. Similar to the case of NO, g_{zz} is the component more sensitive to the surface crystal field of the cationic site causing the Δ splitting. In the bottom of Fig. 4 a TEM picture of polycrystalline CaO materials. This solid

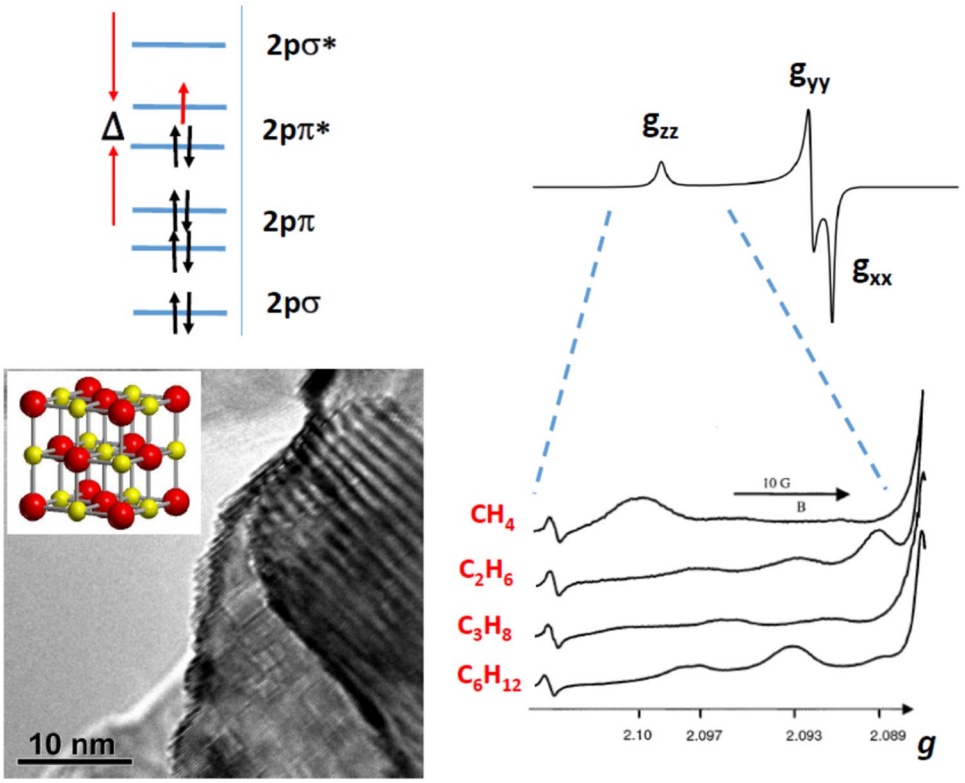

Fig. 4 Top: M.O. scheme of the 13e⁻ adsorbed superoxide O_2^- radical and simulated trace of a generic EPR signal of this species. Bottom: TEM image of polycrystalline CaO and magnification of the g_{zz} region of the superoxide signal obtained by co-adsorption of oxygen and four different alkanes or cycloalkanes (see text)

has been contacted with four different hydrocarbons (methane, ethane, propane and cicloexane) mixed with molecular oxygen. In all these cases no reaction is observed adsorbing the various mixtures on MgO whereas an appreciable amount of superoxide $O_2^{-}{}_{(ads)}$ is produced by contact with CaO showing that at the surface of this oxide highly basic O^{2-} sites are present capable of proton abstraction from these extremely stable molecules. Interestingly the spectral profile in the g_{zz} region, magnified in the bottom of Fig. 4, differs in the four cases indicating that the sites where electron transfer occurs are not the same.

3.2.2 The $O^{\cdot-}$ Ion and the Homolytic Splitting of H–H and C–H Bond

While basic O^{2-} ions are able, as shown before, of H^+ abstraction from R–H (or H–H) bonds, the $O^{\cdot-}$ radical ions induce homolytic splitting of the same bonds with abstraction of H atoms.

The electron configuration of the $O^{\cdot-}$ ion is [$2px^2$, $2py^2$, $2pz^1$] and the corresponding g tensor [43], in a simplified form and in the common case of an axial symmetry of the crystal field, can be written as

$$g_{zz} = g_{||} \approx g_e; \quad g_{xx} = g_{yy} = g_{\perp} = g_e + 2\lambda/\Delta E \tag{8}$$

where λ is the spin–orbit coupling constant for atomic oxygen and ΔE the energy splitting shown in Scheme 1.

The $O^{\cdot-}$ ion can be seen as an oxide ion trapping a hole. For this reason, this radical ion plays a fundamental role in photocatalysis processes. The initial step of a photocatalytic process is the light induced charge separation occurring in a semiconducting oxide (or in analogous systems) caused by photons. The absorption of photons with energy higher than the band gap causes the promotion of electrons from the valence band (VB) to the conduction band (CB) leaving behind a hole, according to the equation:

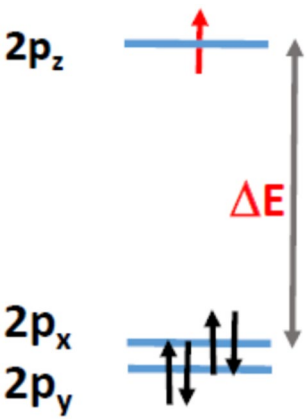

Scheme 1 Energy levels of the $O^{\cdot-}$ radical ion (in axial symmetry)

$$MO + h\nu \rightarrow h^+_{(VB)} + e^-_{(CB)} \tag{9}$$

After the excitation two opposite processes compete, that of charge recombination (detrimental for photocatalysis) and that of charge migration. In the case of semiconducting oxides used in photocatalysis when the photoexcitation experiment is carried out under vacuum a fraction of the photogenerated carriers can be observed by EPR either under continuous irradiation or after irradiation provided that the temperature is kept low enough to prevent recombination. An example is shown in Fig. 5 in the case of titanium dioxide. This oxide had the prominent role in the development of photocatalytic studies and it is still a benchmark in catalytic research. In the case of Fig. 5 the experiment concerns anatase, one of the three main polymorph of this oxide. The solid in the dark shows a nearly flat base line (Fig. 5a). The positive holes tend to localize on the oxygen ions (O^{2-}) of the lattice forming a paramagnetic $O^{\cdot-}$ ion

$$O^{2-} + h^+ \rightarrow O^{\cdot-} \tag{10}$$

whose typical signal is observed at $g > g_e$, (low magnetic field in Fig. 5b) according to Eq. 8. The photogenerated electrons are trapped on a metal cation sites producing trivalent

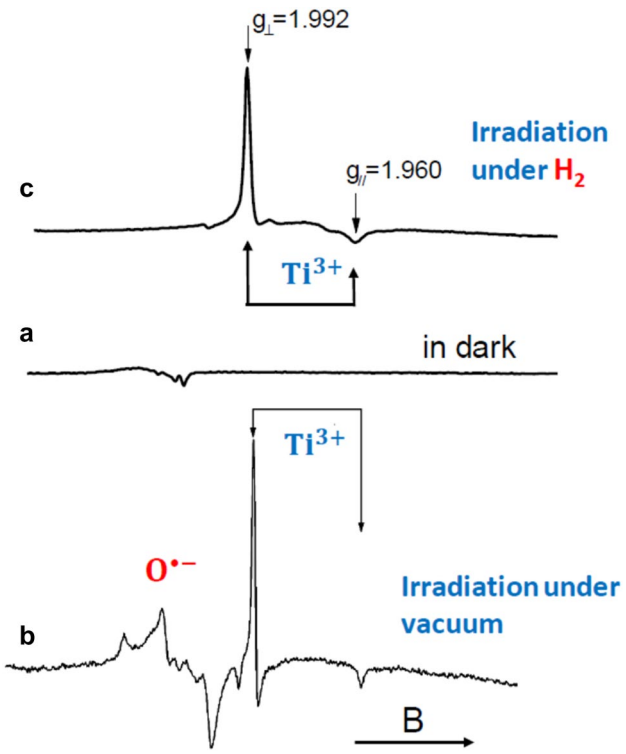

Fig. 5 Effect of UV irradiation on TiO_2 anatase. **a** EPR spectrum in the dark; **b** irradiation under vacuum; **c** irradiation under hydrogen atmosphere

titanium ions whose axial EPR signal [44] is observed at higher magnetic field in Fig. 5b.

$$Ti^{4+} + e^- \rightarrow Ti^{3+} \quad (11)$$

The reactivity of the trapped hole ($O^{\cdot -}$ ions) and the ability in homolytic bond cleavage is shown performing the same type of irradiation under a hydrogen atmosphere. In this case the photoformed holes moving in the crystal reach the surface entailing the following series of reactions based on the ability of the surface hole centre ($O^{\cdot}$) to cause the homolytic splitting of H_2 generating reactive hydrogen atoms [45]

$$h^+_{(VB)} + O^{2-}_{(surf)} \rightarrow O^{\cdot -}_{(surf)} \quad (12)$$

$$O^{\cdot -}_{(surf)} + H_{2(gas)} \rightarrow OH^-_{(surf)} + H^{\cdot} \quad (13)$$

The highly reducing H atoms ionize at the surface transferring their electron to cationic centres of the solid, Ti^{4+} ions, whose reduction is monitored by EPR (Fig. 5c).

$$H^{\cdot} + O^{2-}_{(surf)} + Ti^{4+} \rightarrow OH^-_{(surf)} + Ti^{3+} \quad (14)$$

The EPR signal of Ti^{3+} in Fig. 5c is therefore due to the combined effect of both photogenerated electrons, that are directly trapped by Ti^{4+} ions (Eq. 11), and photogenerated holes that operate through the mechanism described in Eqs. 12–14.

The reported example illustrates the particular role played by EPR in the investigation of photocatalytic processes. Since these are based on an initial event of charge separation and on a series of sequential charge transfer reactions, paramagnetic species are generated in all steps making photocatalytic phenomena an excellent playground for the applications of EPR.

Another important example involving surface $O^{\cdot -}$ centres, that sparked a lot of interest in the catalytic community in the past, is the oxidative coupling of methane first reported by J. Lunsford and co-workers using a lithium promoted MgO catalyst (Li-MgO) and based, according to the Authors, on the reactivity of surface Li^+–$O^{\cdot -}$ centers [46]. The presence of $O^{\cdot -}$ in this solid is ascribed to the valence induction caused by the insertion of the aliovalent Li^+ in the MgO matrix. The stoichiometry of this system can, in principle, be written as $Li^+_x Mg^{2+}_{1-x} O^{2-}_{1-x} O^{\cdot -}_x$. Surface exposed Li^+–$O^{\cdot -}$ centres in this material have been indicated, on the basis of EPR results, as responsible for the C–H cleavage [47] according to

$$CH_{4(g)} + O^-_{(surf)} \rightarrow \cdot CH_{3(g)} + OH^- \quad (15)$$

The Li^+–$O^{\cdot -}$ center are however rather elusive and the authors claim they exist in equilibrium state only at high temperature in the presence of oxygen. The resultant methyl radicals have been isolated using a matrix isolation technique at low temperature [48]. In catalytic conditions methyl radicals are either released in the gas to form ethane by radical coupling or trapped at the surface as methoxy species

$$\cdot CH_3 + O^{2-} + O_2 \rightarrow CH_3O^- + O_2^{\cdot -} \quad (16)$$

that entail a complex series of reactions, whose main products are ethane and carbon oxides.

The same Li–MgO system was revisited some years later in a thorough study on both films and powdered samples [49]. The features of the system resulted much more complex than previously observed and the solubility of Li^+ was found quite inhomogeneous with formation also of oxygen vacancies and segregation of LiO_x clusters. Li^+–$O^{\cdot -}$ centers, in particular, were not observed, in this case, by EPR.

To this end it has to be kept in mind that paramagnetic species are not necessarily EPR visible in all conditions. This concept is appropriately illustrated by the example concerning Na doped CaO, a system analogous to Li-MgO, consisting in a monovalent dopant incorporated in a alkali-earth oxide matrix [50]. Na-CaO was prepared decomposing a sample of calcium carbonate containing

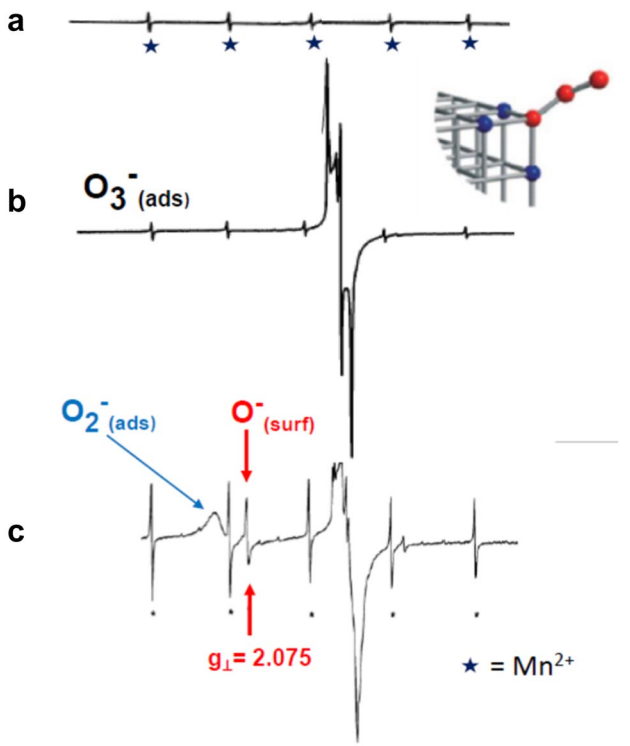

Fig. 6 **a** EPR spectrum at 77 K of the bare Na-CaO material (the stars indicate five of the six Mn^{2+} lines); **b** EPR spectrum at 77 K after adsorption of O_2 (the scheme shows the structural features of the $O_3^{\cdot -}$ adduct; **c** EPR spectrum recorded at 77 K and resulting from the decomposition of the $O_3^{\cdot -}$ by evacuation at 323 K

sodium impurities and, after decomposition, it shows an EPR spectrum with a flat base line except for the presence of a weak sextet of hyperfine lines due to traces of Mn^{2+}, unavoidably occurring in calcium oxide (Fig. 6a). In Na-CaO the aliovalent Na^+ ions are actually compensated by $O^{\cdot -}$ centres that are not, however, EPR-active ($Na^+_xCa^{2+}_{1-x}O^{2-}_{1-x}O^{\cdot -}_x$) as they do not appear in the EPR spectrum of Fig. 6a. Their presence is however revealed by adsorption of molecular oxygen at low temperature. In such conditions the intense signal shown in Fig. 6b shows up which is due to the formation of ozonide $O_3^{\cdot -}$ ions [51], whose **g** tensor elements are well known. The ozonide species is formed according to a simple addition of molecular oxygen and requires the presence of $O^{\cdot -}$ at the surface:

$$O^{\cdot -}_{(surf)} + O_{2(gas)} \leftrightarrows O^{\cdot -}_{3\,(ads)} \tag{17}$$

It is worth mentioning that the same reaction is not observed in the case of undoped CaO and MgO that do not react with molecular oxygen. The ozonide adduct is unstable and decomposes rising the temperature. Remarkably, by a careful control of the experimental conditions (gentle vacuum annealing at 323 K and immediate quenching at 77 K) it has been possible to monitor an intermediate step of $O_3^{\cdot -}$ decomposition that leads to the formation of two new, partially overlapped, EPR signals. The former is due to a superoxide $O_2^{\cdot -}$ adsorbed on Ca^{2+} (whose distinctive features is the g_{zz} component at 2.10, (Fig. 6c) while the second is due to the perpendicular component of a $O^{\cdot -}$ signal having $g_\perp = 2.075$ as confirmed by a separate experiment of CaO irradiation by X ray with evidence of trapped electrons and trapped holes [50].

The $O^{\cdot -}$ species is observed in a restricted time interval since it progressively disappears upon prolonged annealing confirming its nature of elusive species. The decomposition mechanism of the oxonide ion is complex involving at least two distinct reaction channels. The whole stoichiometry is summarized by the following equation

$$3O^{\cdot -}_3 \rightarrow 2O^{\cdot -}_2 + O^{\cdot -} + 2O_2 \tag{18}$$

The reason of the non-detectability of the $O^{\cdot -}$ radical ion in Na-CaO is not fully clear. It has to be recalled, however, that all experiments reporting a hole center in an oxide matrix concern cases of relatively low symmetry of the environment as it occurs in correspondence of a cation vacancy (the V centers [52] described in solid state physics) or at the surface of a solid. A tentative explanation considers that in case of a highly symmetric environment of the defect centre (small or nearly null ΔE value in Eq. 8) the resonance is expected to cover a wide range of magnetic field and its signal becomes practically undetectable. To conclude, the $O^{-\cdot}$ defect in Na-CaO is likely highly mobile and undetectable when moving in the volume of the crystal. The effect of oxygen adsorption is to trap the defect at the surface with formation of a rather labile ozonide ion stable in a limited range of temperature and oxygen pressure on the basis of the equilibrium reaction reported in Eq. 17.

3.3 Chemical Bonding at Solid Surfaces

3.3.1 Probing the Nature of the Metal-Oxide Chemical Bond

When the interaction between an adsorbate and a surface site produces a paramagnetic entity, the EPR technique can be extremely powerful in describing in detail the features of the chemical bond occurring at the surface. We will discuss this point using two examples from the literature. The former one concerns the bonding between single metal atoms and the surface of an oxide. It is well known in fact that, in principle, the catalytic properties of a given metal are conditioned by the interaction of the latter with the support (usually an oxide). By evaporation of alkali metals (Na, K, Rb, Cs) in contact with the surface of polycrystalline MeO (Me = Mg, Ca, Sr) the initial observed interaction leads to metal ionization and formation of surface trapped electron centers. However higher amounts of metal vapor produce paramagnetic centers characterized by a distinctive hyperfine structure typical of alkaline metals (all having non zero nuclear spin). We will discuss here in particular the case of potassium (^{39}K, $I = 3/2$, abundance = 93.6%).

The observed centers in this case contain a single metal atom since the signal consists in four lines arising from the hyperfine interaction of the unpaired electron with the nucleus of ^{39}K. The spectrum is reported in Fig. 7 (K-MgO) and its structure is prevalently isotropic indicating the s character of the unpaired electron orbital (Fermi contact, see Sect. 2) with only some minor anisotropic contribution which causes a small distortion of the spectral structure.

The most relevant feature of this spectrum is the reduction of the hyperfine separation that drops out of about one half with respect to that of the free atom in the gas phase (4.14 mT vs. 8.23 mT) that is also reported in Fig. 7 (red trace). An initial hypothesis [53] of a partial delocalisation of the $4s^1$ electron spin density onto trapping sites of the solid surface was rejected by successive investigations employing MgO surface-enriched in ^{17}O [54] which is the only O isotope bearing a non zero nuclear spin ($I = 5/2$) and has ben inserted on the surface by exchange with $H_2{}^{17}O$. The EPR spectrum of the monomeric center interacting with the isotopically enriched surface shows the onset of an additional sextet spaced by 0.28 mT on each K line proving that the metal atom is bound to surface oxygen ions with, however, a tiny degree of electron delocalisation towards the

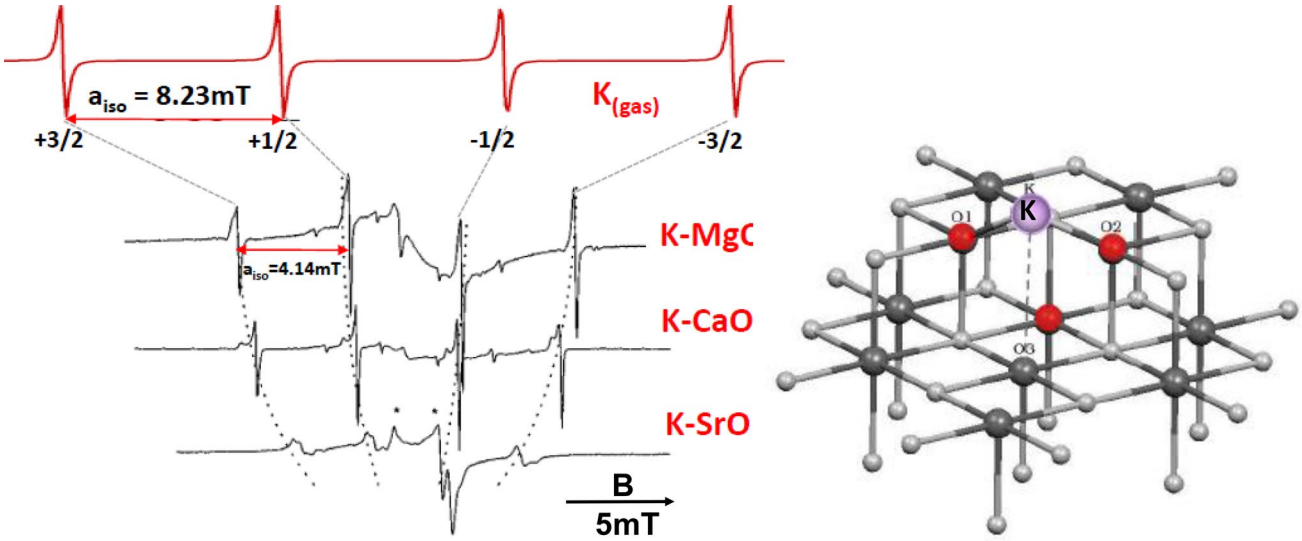

Fig. 7 EPR spectra of mononuclear species obtained upon contact of potassium vapors with the surface of polycrystalline MgO, Cao and SrO. The EPR spectra are compared with that of potassium in the gas phase (red trace, computer simulation). At the right hand side of the figure the scheme of K adsorbed at the reverse corner morphological defect of MgO

adsorbing site, not accounting for the observed lack of electron spin density with respect to the isolated atom. Further analysis by HYSCORE demonstrated that the single K atom interacts with at least three surface oxide anions. The model derived from this experimental finding involves a strong perturbation of the unpaired electron wave function caused by the polarizing interaction of the O^{2-} lone pairs with the 4*s* orbital containing the K valence electron. This interaction destabilizes the latter orbital leading to an "expanded" atom structure reminiscent of a Rydberg state, with a sort of matrix-induced nephelauxetic effect. The Fermi contact term of the expanded $4s^1$ orbital, whose energy is now mid-way between those of 4s and 5s orbitals of the unperturbed atom, dramatically decreases with respect to that of gas phase potassium without an effective electron delocalisation. This achievement could not have been fully acquired without the essential contribution of advanced theoretical calculations that corroborate this view and allowed the identification of a surface site involving three oxide ions with suitable geometry. This is the reverse corner site at the intersection with two perpendicular steps shown in Fig. 7. In this case the structure of the computed tensors confirms the drop of K hyperfine and the nature of the bonding. Furthermore, the calculated interaction energy (1.11 eV) is in line with the observed stability of the monomeric species up to room temperature. The molecular orbital scheme of the described surface interaction is illustrated in Fig. 8. The same type of phenomenon was observed in the case of K evaporation onto CaO and SrO. Interestingly, with increasing the basicity of the oxide (e.g. the donating ability of the O^{2-} lone pairs) the polarizing effect increases and the ^{39}K hyperfine constants further drop (Fig. 7) showing a linear correlation with the optical basicity of the three oxides [54].

The described bonding scheme is not limited to alkaline metals but it can be extended also to metals of higher interest for heterogeneous catalysis such as gold. The deposition of Au single atoms on the (001) surface of a MgO thin film enriched in ^{17}O was investigated by Freund et al. [55] monitoring the interaction by the joint use of EPR and STM. Gold exhibits an electronic configuration analogous to that of alkaline metals ([Xe] $4f^{14}$ $5d^{10}$ $6s^1$). A large reduction of the ^{197}Au ($I=3/2$) hyperfine coupling constant was observed upon deposition on MgO while the angular dependence of the ^{17}O superhyperfine lines suggested the stabilisation

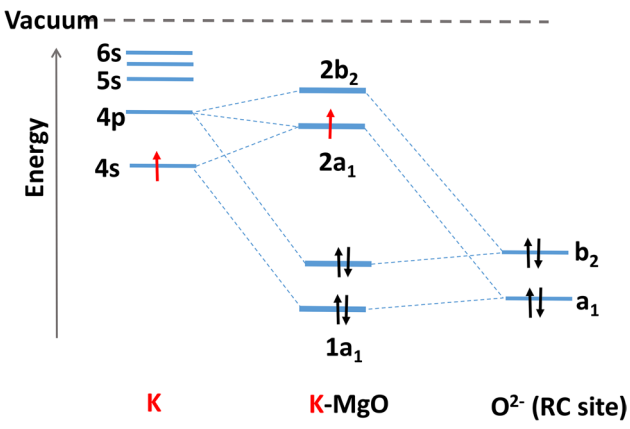

Fig. 8 The molecular orbital scheme of the bonding of a K atom at the reverse corner morphological defect at the MgO surface

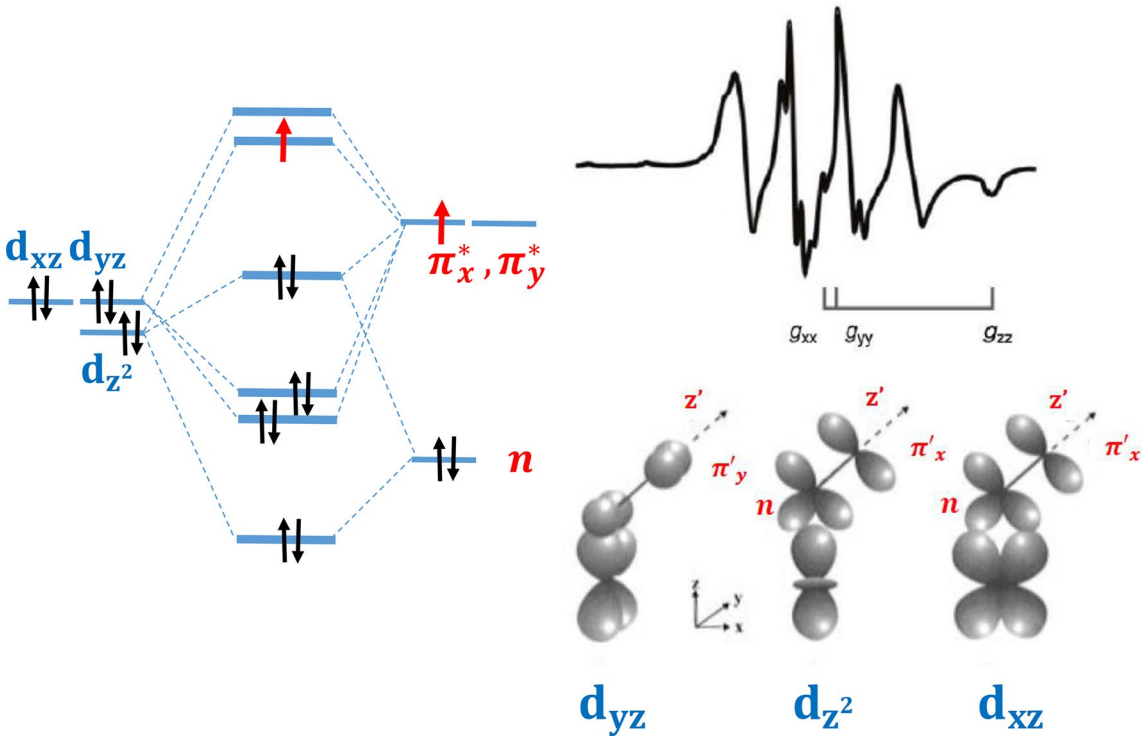

Fig. 9 Left: MO scheme of the bonding of NO with a Cu^+ ion. Right: CW-EPR spectrum and (bottom) picture of the relevant orbital interactions of the $[CuNO]^+$ adduct in ZSM-5 zeolite

of the metal atom on top of a single O^{2-} ions of the (001) surface. Theoretical calculations confirm the idea that the large decrease of the isotropic hyperfine contact is not due to electron delocalisation but, rather, to a complex interplay between some degree of covalence (hybridisation of Au 6s and 5d with O 2p orbitals) and a pronounced polarisation of the 6s spin density, analogous to that described before for K on polycrystalline MgO [54]. Concerning the subject of metal atoms on solid surfaces it is worth mentioning that recently, electron magnetic resonance combined with scanning tunneling microscopy (STM) achieved single-spin sensitivity with sub-angstrom spatial resolution. EPR-STM has been successfully used for the study of magnetic properties and interactions of individual transition metal atoms (Ti, Fe) adsorbed on MgO [56–58].

A case somehow parallel to that described above was followed investigating the interaction of Zn and Cd monovalent ions (both paramagnetic having ns^1 configuration) with the framework of a ZSM-5 zeolite enriched with ^{17}O via a series of hydration-dehydration cycles using water vapour enriched with $H_2{}^{17}O$ [59]. These two metal ions have been recently considered as active centres in the activation of small hydrocarbon molecules [60, 61]. The interaction of Zn^+ and Cd^+ with the framework is investigated monitoring the ^{17}O hyperfine by X-band CW-EPR and Q-band HYSCORE. Zn^+ coordinates to two equivalent oxygen atoms forming an adduct with pseudo C_{2v} symmetry while the equivalent Cd^+ is less symmetric with two non-equivalent framework oxygen. Coupling these results with DFT modelling it was possible to individuate the framework sites where the interaction occurs. The picture of the interaction between the two monovalent cations of Group XII and the zeolitic framework is different than in the previous case (K-MgO) since about 10% of the electron spin density originally present on the ns^1 systems is transferred onto the lattice oxygen to form a chemical bond with ionic-covalent character. As it will be illustrated in the following of the present paper, ^{17}O labelling is becoming an extremely powerful tool to explore the chemical bonding in oxide-based catalytic systems.

3.3.2 Chemical Bonding in Surface Adducts of Transition Metal Ions

Isolated transition metal ions incorporated in the framework of zeolites have an utmost importance in modern catalysis. For example, 30 years after the first reports on nitric oxide decomposition on Cu^{2+}-exchanged zeolites [62, 63], this subject remains a highly current topic in research [64]. Central aspects of the catalytic chemistry of these materials are both the transformation of Cu^{2+} sites in Cu^+ and the features of the chemical bond in the reaction intermediates between NO and the cuprous ions that are critical to explain

the catalytic action [65]. As to the latter aspect, EPR have played in the past an important role due to its intrinsic ability to unravel details of the chemical bonding when paramagnetic species are involved. In particular, the nature of the interaction between Cu^+ ions and NO in Cu-ZSM5, widely investigated in the past, is briefly mentioned here to illustrate the delicate balance between donation and back-donation operating in these transition metal adducts. When NO is contacted with a pre-reduced material mainly containing Cu^+, an intense spectrum is observed by CW-EPR (Fig. 9) which is characterized by hyperfine interactions due to [63, 65] Cu nuclei, both having $I=3/2$, and to ^{14}N ($I=1$) [66].

Simulation and analysis of the spin-Hamiltonian parameters allowed to unravel the features of a Cu^+NO species with η^1bent structure and characterized by monoclinic symmetry, e.g. the non-coincidence of the axes of $\boldsymbol{g}$ and $\boldsymbol{A}$ tensors. The main fraction of the electron spin density is localized on the coordinated NO molecule with, however, a relevant degree of delocalisation from the π antibonding NO orbital onto copper orbitals through the bond drafted in Fig. 9 [67]. This is based on the overlap of Cu^+ $3d_{z2}$,$3d_{xz}$ and a lone pair N orbital (n) with a NO $2\pi^*$ which determines the SOMO, while the interaction of $3d_{xy}$ and the other NO $2\pi^*$ originates the LUMO. The large value of the isotropic component of the hyperfine constant (Fermi contact) is due to both the spin polarisation of inner Cu s-orbitals and to a contribution of spin delocalisation onto the 4s one. The total spin densities are about 0.2 for copper, 0.55 for nitrogen. The remaining spin density (0.25), not accounted for by the EPR spectrum, is on oxygen. The described nitrosyl adduct is rather labile and can play a role in further NO reactivity. It has been hypothesized in fact that an electrophilic attack of a second molecule in the gas phase to the activated nitrosyl leads to the formation of a N–N bond, essential step for the direct decomposition of nitric oxide. Successive experimental work using multifrequency EPR and pulse EPR has further contributed to the characterisation of this important intermediate [68, 69] while advanced computational investigations have nicely confirmed and further detailed the picture of the chemical bond derived from EPR [70–72].

This bonding interaction is of relevance in the context of the abatement of NOx pollutant where nickel-exchanged zeolite catalysts have also received a considerable scientific interest due to their capability to promote the HC-SCR reaction with both unsaturated and saturated hydrocarbons, comprising methane [73]. In this context, the mechanistic aspects of model selective catalytic reduction (SCR) of NO with C_2H_4 over Ni/ZSM-5 zeolite were recently investigated by means of advanced correlation EPR/HYSCORE methods, revealing fine details of the electronic and magnetic structure of Ni^{2+}–NO [74].

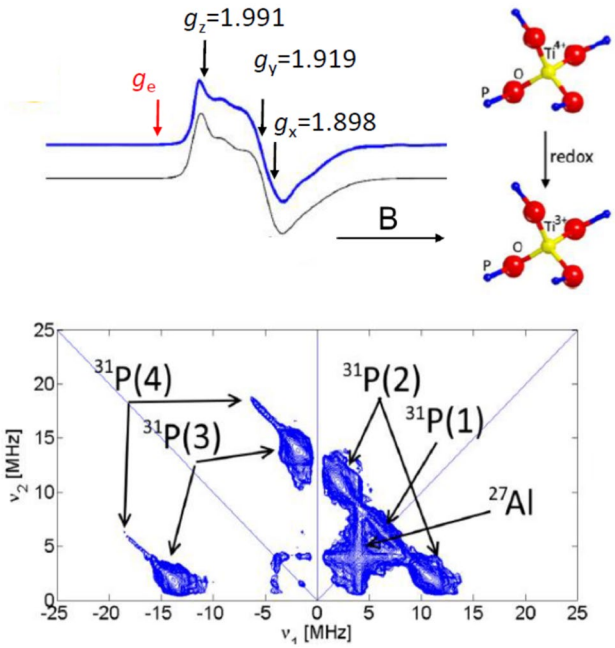

Fig. 10 Top: CW-EPR spectrum of Ti^{3+} in hydrogen reduced Ti-AlPO and scheme of the catalytic site. Bottom: HYSCORE spectrum of Ti^{3+} in the AlPO framework

3.4 Topological Description of Active Sites in Catalytic Systems

The potential of EPR techniques in the investigation of heterogeneous catalysts is primarily related to the observation of hyperfine and superhyperfine interactions with the surroundings. CW-EPR has an intrinsic limitation in this context since the interaction between electron and nuclear magnetic moments are usually resolved when they are large enough in comparison with the intrinsic linewidth of the signal. This implicates that superhyperfine interactions with the first coordination sphere of the paramagnetic centre, and a fortiori with the second sphere, are seldom detected by CW-EPR. The advent of pulsed methods in EPR has open new perspectives in this area since the magnitude of detectable hyperfine splitting is comparable to NMR resolution. To this end the two following examples are paradigmatic. Both concern subtle structural and topological aspects of two important catalytic systems whose features have been disclosed using pulsed EPR and, in particular, the so called hyperfine techniques.

3.4.1 Open Framework Systems

Aluminophosphates molecular sieves (AlPOs) are a family of zeotype materials [75] that, more easily than aluminoslilicates, can incorporate transition metal ions into their framework giving origin to new materials with high

potential for applications in heterogeneous catalysis. The neutral network of AlPOs is made up by connected tetrahedral units of AlO_4 and PO_4. Particularly interesting is the case of the incorporation of Ti^{4+} ions that adds the redox properties typical of the transition ion to the acidic ones typical of the AlPO-4 network [76]. Several questions have been debated in the literature about this system, in particular concerning the site of isomorphous substitution (P or Al), the role of Ti ions in redox chemistry and their availability to coordinating molecules. EPR techniques have played a crucial role in this debate. The system is in fact reducible and by thermal treatment at 673 K in hydrogen atmosphere the EPR signal of a Ti^{3+} ions shows up as illustrated in Fig. 10. The reduction of Ti^{4+} is accompanied by stabilisation of an H^+ by an oxygen of the network to maintain the electric neutrality.

$$Ti^{4+} + O^{2-} + 1/2\ H_2 \rightarrow Ti^{3+} + OH^- \quad (19)$$

Due to the low abundance of isotopes with $I \neq 0$ no Ti hyperfine is usually observed in Ti^{3+} powder spectra and the information is limited to the $\boldsymbol{g}$ tensor. However the dependence of the $\boldsymbol{g}$ tensor on the symmetry of the environment is well known [18, 19, 77] and the nearly axial signal in Fig. 10 is unambiguously associated to ions in the tetrahedral crystal field of four oxygen atoms thus showing that titanium ions are indeed incorporated in the AlPO framework. The specific location of the reduced ion however does not show up from the CW spectrum. The two possible situations imply a difference in the second coordination sphere that is composed by Al ions in the case of isomorphous substitution at the P site and vice-versa. Both ^{27}Al ($I = 5/2$) and ^{31}P ($I = 1/2$) have 100% natural abundance but the tiny superhyperfine interaction with the unpaired electron on Ti^{3+} is not perceptible in the CW spectrum characterized by the large linewidth typical of transition metal ions. The problem was faced using HYSCORE. The spectrum reported in the bottom of Fig. 10 shows the cross peaks ascribable to the interaction of the unpaired electron with four distinct ^{31}P nuclei [78]. The only trace due to ^{27}Al is due to remote nuclei.

This experiment therefore demonstrates that titanium ions are actually inserted in the tetrahedral framework and, additionally, that the reducible titanium ions are those replacing Al in the ALPO network (Scheme in Fig. 10, top). The ^{31}P coupling constants measured in the HYSCORE experiment range from 10 to 30 MHz and, as expected, are too small to be directly observed by CW-EPR. The tetrahedral Ti^{3+} ions are coordinatively unsaturated and their coordination sphere is modified by adsorption of Lewis bases such as water and ammonia. In this latter case two NH_3 ligands bind to the catalytic centre whose hyperfine and quadrupole ^{14}N coupling tensors have been fully resolved [79]. The same approach here illustrated was also followed for the characterisation of vanadium centres in the framework of monometallic VAlPO-5 [80] and bimetallic VTiAlPO-5 catalysts with relevant catalytic activity and selectivity in aerobic oxidations [81]. In this case, HYSCORE and EPR were key to demonstrate that well-defined and isolated oxophilic tetrahedral titanium centers coupled with redox-active VO^{2+} ions at proximal framework positions provide the loci for the activation of oxidant that boosts the catalytic activity compared to analogous monometallic systems.

3.4.2 Ziegler–Natta Catalysts

Ziegler–Natta (Z–N) systems for the production of polyolefines are highly effective catalysts that, in spite of a great deal of investigations and of about 60 years of industrial application, remain rather elusive. ZN catalysts are very complex systems whose main components are titanium ionic species generated adsorbing a precursor (most often $TiCl_4$) on the surface of magnesium dichloride. The catalyst however needs of a cocatalyst (usually an aluminium alkyl) that reduces the adsorbed Ti species producing in this way the active sites for the polymerisation reaction. EMR techniques, coupled with DFT calculations, have contributed to shed some light on the nature of surface reduced Ti species present at the surface of an activated Z–N catalyst.

An early report by Schmidt et al. [82] has been, at the same time, the first EPR study of the surface of a single crystal and the first surface science investigation of a Ziegler–Natta catalyst. A (001) crystal face of $MgCl_2$ was prepared by evaporation employing a Knudsen cell. $TiCl_4$ could be adsorbed on this surface only after increasing the defect density by ion bombardment and reduced Ti^{3+} centers were so observed by EPR. The system however becomes catalytically active only after interaction with aluminium alkyl ad shown by the direct EPR detection of ethyl radical by EPR.

X-band continuous wave (CW) EPR techniques have been largely used in the characterization of real ZN catalysts primarily to monitor and quantify the amount of reduced Ti species [83–85]. In the case of supported titanium–magnesium catalysts with a low titanium content (≤ 0.1wt%), isolated mononuclear Ti(III) species have been reported to form on the surface at a high yield (40–70% of the total titanium content). Moreover, a correlation was found between the content of the isolated Ti(III) species and the activity of these catalysts in ethylene polymerization [86]. The observed g values for activated ZN catalysts depends on many factors, including the presence of coordinated AlR_3 co-catalysts, the potential coordination of Lewis basis and the localization at different surface terminations of the $MgCl_2$ support. Tregubov et al. [87] reported spectra with two Ti(III) signals

with axial **g** tensor ($g_{\perp}^{1} = 1.984$, $g_{\perp}^{2} = 1.966$ and $g_{\parallel}^{1,2} = 1.79$) for a supported $TiCl_4/MgCl_2$ system obtained by the reduction with triisobutylaluminium (TIBA). EPR spectra of the $TiCl_3 \cdot 0.3AlCl_3$ catalyst showed a signal with $g_{\perp} = 1.94$ and $g_{\parallel} = 1.90$ (with a concentration of just 1% of the total titanium content) [88].

More recently CW and pulse-EPR were applied to investigate the surface of a fourth generation Z–N catalyst. A $MgCl_2/TiCl_4$/dibutylphtalate precatalyst (2% Ti by weight) was treated in situ with triethylaluminium (TEA) vapors and invesigated by EMR following a multifrequency approach [89]. The intense EPR spectrum, due to Ti^{3+} centers, observed upon this treatment concerns some 15% of the total titanium content. Despite the complexity of the catalytic system the EPR spectrum is well defined and can be interpreted, according to the computer simulation, as the overlap of two main Ti^{3+} signals (Fig. 11a) corresponding to two distinct surface sites. HYSCORE experiments show that Ti^{3+} centres are coordinated to Cl atoms as shown by the ridges in Fig. 11a′ related to the interaction with ^{35}Cl and ^{37}Cl both having I = 3/2. $TiCl_3$ molecular complexes are therefore formed, compatible with the location on $MgCl_2$ (110) faces as indicated by DFT modelling. The accessibility of such sites (an important parameter to unravel the nature of catalytically active sites) was tested by adsorption of oxygen with consequent electron transfer and formation of superoxide $O_2^{\cdot -}$ radical ions stabilized on top of Ti^{4+} (Fig. 11b) whose signal is well known. Oxygen reacts with about 60% of the Ti^{3+} ions generated at the surface. The remaining centers are therefore not exposed at the surface. The EPR analysis of the Ti^{3+} centres however, does not provide any information about the TEA co-catalyst although this contains Al nuclei with non-zero nuclear spin. To this end, the $O_2^{\cdot -}$centres constitutes a second paramagnetic probe to be exploited for a further monitoring of the environment. Remarkably Q-band HYSCORE shows two ^{27}Al cross peaks (Fig. 11b′) indicating a direct interaction of this radical with an Al ion. The above results as a whole, resumed by the pictorial scheme in the Figure, represent an important step in the search of a satisfactory description of a highly important however elusive catalytic system. Following this first report, the use of advanced EPR techniques in this field has been successfully applied to investigate molecular complexes and surface species for olefines polymerization [90–93].

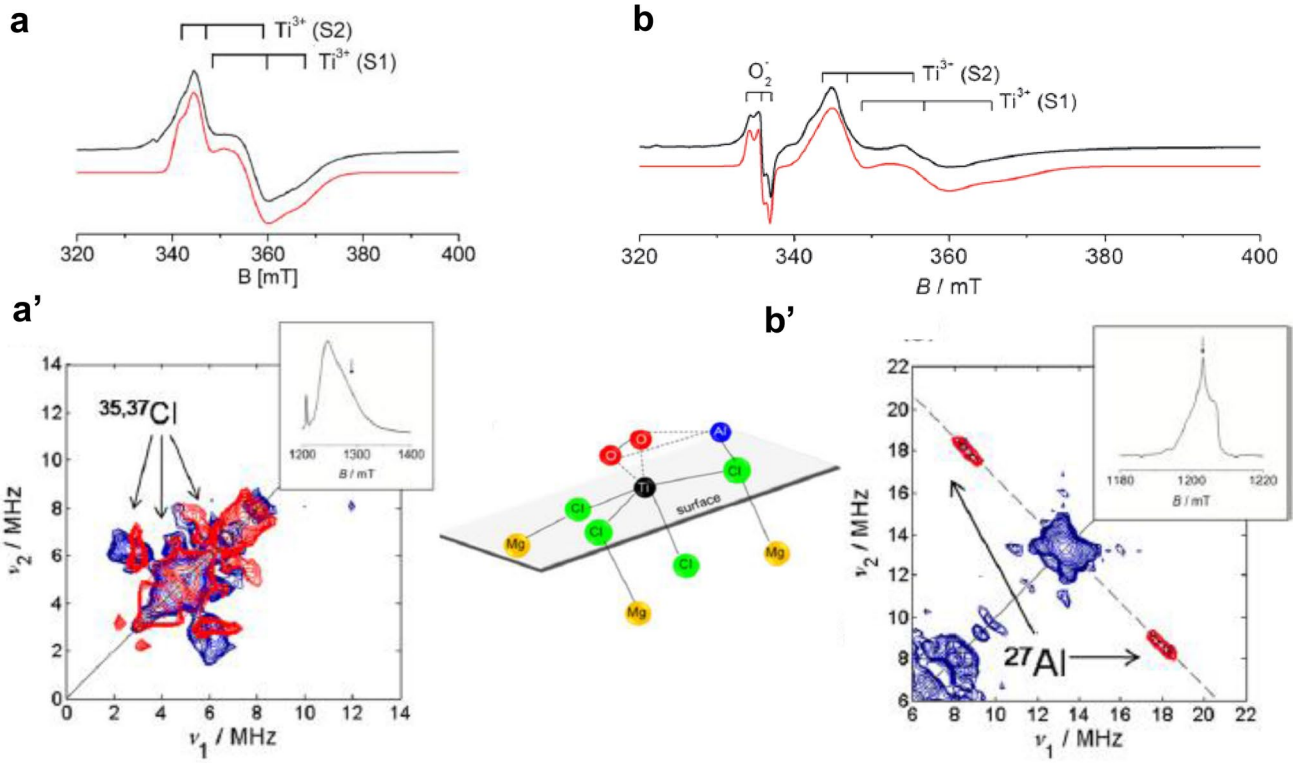

Fig. 11 Top: X-band CW-EPR spectra of the activated Z–N catalyst before (**a**) and after (**b**) contact with O_2. Bottom: HYSCORE spectra showing the hyperfine interaction of Ti^{3+} with Cl (**a**′) and that of O^{2-} with Al. The scheme report the structure of the whole centre as derived by EMR

3.5 Geometrical and Electronic Structure of Catalytic Sites Via Selective Isotopic Enrichment

An obvious mandatory conditions for the observation of hyperfine structures in a EPR spectrum is the presence of "magnetic" nuclei ($I \neq 0$) in the chemical environment of the paramagnetic centre. The isotopic composition of oxygen in natural abundance is dominated by nuclei with $I = 0$ (^{16}O, 99.76% and ^{18}O, 0.2%) while ^{17}O, with $I = 5/2$, represents a fraction of about 0.04% only, with absolutely no chance to produce a detectable hyperfine structure in EPR spectra. This fact constitutes a severe limitation in catalytic studies considering the dominant role of oxygen in the composition of heterogeneous catalytic systems. Initially, and for several years, the ^{17}O isotopic labelling was limited to the use of enriched gaseous oxygen [38] to characterize the structural features of surface adsorbed species. Only more recently our group started a more systematic effort of incorporating the isotope at the surface [94] or in the bulk [95] of the investigated oxide materials as it has been also shown, for instance, in the examples reported in Sect. 3.3.

The joint use of ^{17}O isotopic labelling and pulse-EPR technique (that extend the monitoring to weak electron–nuclear interaction viz. to atoms more distant from the paramagnetic centre) represents a tremendous improvement of quality in catalytic research by EMR methods. The following example, concerning a system obtained by evaporation of VCl_4 onto the framework of a H-ZSM-5 zeolite [96], illustrates the potential of this approach in terms of structural characterisation of a catalytic site.

CW-EPR spectra (Fig. 12 top) suggest the presence of isolated vanadylic VO^{2+} species formed upon dechlorination of the precursor and provide the measure of the ^{51}V hyperfine structure. Q-band HYSCORE experiments allow to measure the weaker hyperfine interactions with both ^{27}Al (Fig. 12 bottom, revealing the nature of the zeolite framework site of V grafting) and ^{1}H (unravelling the presence of a hydroxyl group in the coordination sphere of the metal).

The atomistic description of the catalytic site, however, is exhaustive only including the information about the framework oxygen in direct interaction with the vanadium centre. This was achieved introducing ^{17}O in the zeolite by preliminary cycles of hydration–dehydration performed using ^{17}O enriched water.

^{17}O incorporation selectively occurs at the active sites and allows the measure of well resolved ^{17}O HYSCORE spectra once that the reaction with VCl_4 has been performed. In this

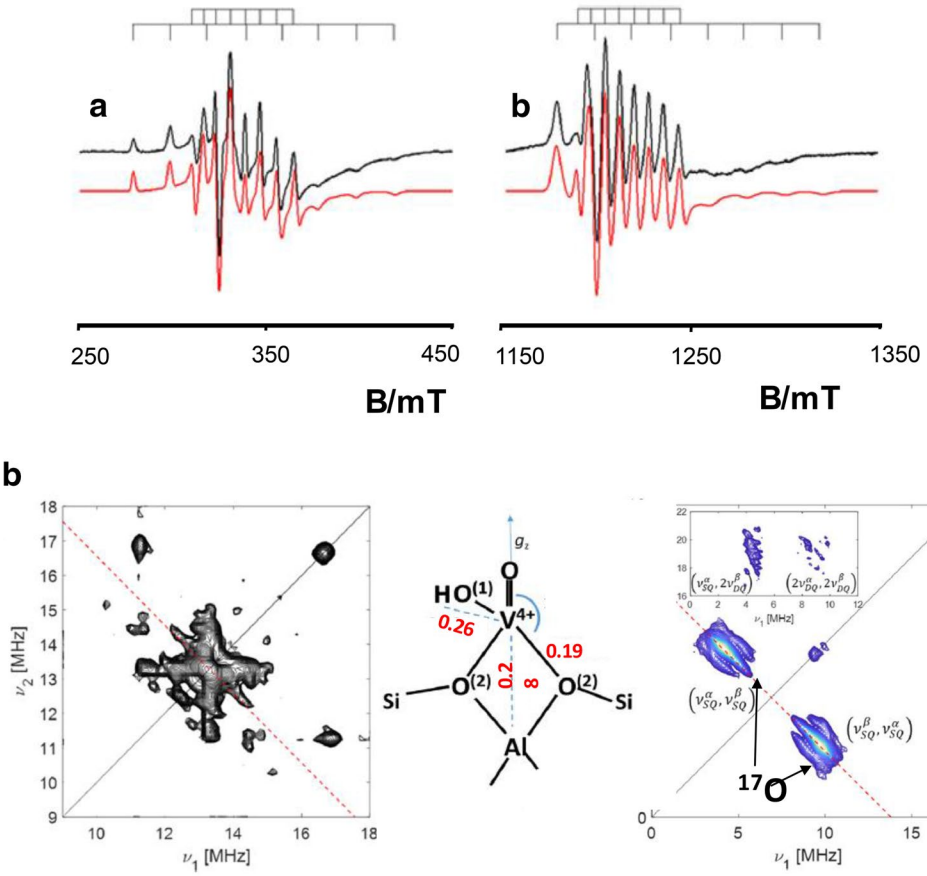

Fig. 12 Top: X-band (left) and Q-band (right) CW-EPR spectra of the vanadylic centres in ^{17}O enriched ZSM-5 zeolites prepared by evaporation of VCl_4. Bottom: HYSCORE spectra monitoring ^{27}Al (left) and ^{17}O hyperfine interaction and structural scheme of the catalytic centre

way the full set of hyperfine constants related to the first and second coordination sphere of Vanadium are obtained allowing to derive a thorough structural model of the centre (bond lengths and bond angles, Fig. 12) rivalling in terms of details with those derived from X-ray techniques. This example definitely shows the enormous potential, in terms of structural description, resulting from coupling the whole arsenal of CW and pulse EPR techniques with a selective isotopic enrichment of the solid.

4 Conclusive Remarks

In the present manuscript some of the main aspects of surface chemistry and heterogeneous catalysis that can be conveniently addressed by EMR techniques have been illustrated. We have tried to emphasize, on the one hand, the ability of these techniques in monitoring reaction intermediates that are often labile and low-concentration entities. On the other hand, we have outlined their strength in the structural and electronic characterization of chemical systems at the surface of solids (mainly oxides, zeolites and other porous systems) that is essentially based on the ability to monitor the interactions of the unpaired electron with its atomic environment. However, trying to answer the second question posed in the introduction about the convenience of introducing EPR instrumentations in the arsenal of a modern laboratory of surface chemistry and catalysis, it appears that these are not simply "plug and play" machines, easily exploitable without a deep specific scientific background. To obtain results going beyond simple analytical data (is a given paramagnetic species present in a system?) it is necessary to handle the complex physics of magnetic interactions. Moreover, pulse-EPR experiments are complex and must be carefully designed in advance to obtain significant results whose interpretation is delicate and non-straightforward. Therefore, since EPR instrumentations, and in particular advanced ones, are rather expensive, it can be inconvenient to invest important resources in an EPR tool without the training necessary to exploit its potential to the maximum level.

Working instead with an adequate background, there are clear advantages in having an EPR instrumentation available in an advanced laboratory of surface chemistry and catalytic sciences. In particular, the ability to measure the electron spin density in the catalytic site and in its surroundings, hence obtaining detailed information on the nature of the SOMO, is a resource of invaluable importance that goes directly to the heart of the chemical interaction as in a few other cases only. To this important point we must add another aspect that only partially emerges from the examples illustrated above. It is the coupling between experimental results and advanced computational methods that is particularly fruitful in the case of EMR techniques. Modern DFT methods are now able to produce highly accurate results in the calculation of EPR and NMR magnetic tensors [97] and several quantum chemical packages have made such calculations relatively accessible. The computational approach becomes therefore a further tool that supports the various CW and pulsed techniques and, in particular, it results highly useful when the EPR data alone are not sufficient to select the correct solution among two or more structural hypotheses compatible with the experimental data.

In conclusion, EMR techniques have, like all experimental techniques used in the world of solid surfaces and catalytic sciences, strengths and weaknesses. We have tried to demonstrate in this paper that the strengths are so important, at the present stage of technological developments of the hardware, that a future season of wider use of Electron Magnetic Resonance in these scientific areas can be confidently foreseen.

Funding Open access funding provided by Università degli Studi di Torino within the CRUI-CARE Agreement..

References

1. O'Reilly DE (1960) Magnetic resonance techniques in catalytic research. Adv Catal 12:31–116
2. Adrian FJ (1968) Guidelines for interpreting electron spin resonance spectra of paramagnetic species adsorbed on surfaces. J Colloid Interface Sci 26:317–354
3. Lunsford JH (1972) Electron spin resonance in catalysis. Adv Catal 22:265–364
4. Howe RF (1993) Electron-paramagnetic-resonance spectroscopy of catalytic surfaces. Colloids Surf A 72:353–363
5. Che M, Giamello E (1994) Electron paramagnetic resonance: principles and Applications to catalysis. In: Imelik B, Vedrine JC (eds) Catalyst characterization: physical techniques for solid materials, Plenum Press, New York
6. Goldfarb D (2009) Electron paramagnetic resonance applications to catalytic and porous materials. In: Brustolon M, Giamello E (eds) Electron paramagnetic resonance: a practitioner toolkit, Wiley, Hoboken
7. Sojka Z (1995) Molecular aspects of catalytic reactivity. Applications of EPR spectroscopy to studies of the mechanism of heterogeneous catalytic reactions. Catal Rev Sci Eng 37:461–512
8. Pietrzyk P, Sojka Z, Giamello E (2012) Electron paramagnetic resonance spectroscopy. In: Che M, Vedrine JC (eds) Characterization of solid materials andheterogeneous catalysts, Wiley-VCH Verlag GmbH & Co

9. Morra E, Maurelli S, Chiesa M, Giamello E (2015) Rational design of engineered multifunctional heterogeneous catalysts. The role of advanced EPR techniques. Top Catal 58:783–795
10. Risse T, Hollmann D, Brükner A (2015) In situ electron paramagnetic resonance (EPR)—a unique tool for analysing structure and reaction behaviour of paramagnetic sites in model and real catalysts. Catalysis 27:1–32
11. Spencer J, Folli A, Richards E, Murphy DM (2019) Applications of electron paramagnetic resonance for interrogating catalytic systems in specialist chemical reports. Electron paramagnetic resonance. The Royal Society of Chemistry, London
12. Goldfarb D (2006) High field ENDOR as a characterization tool for functional sites in microporous materials. Phys Chem Chem Phys 8:2325–2343
13. Dinse A, Ozarowski A, Hess C, Schomäcker R, Dinse KP (2008) Potential of high-frequency EPR for investigation of supported vanadium oxide catalysts. J Phys Chem C 112:17664–17671
14. Dinse A, Carrero C, Ozarowski A, Schomäcker R, Schlögl R, Dinse KP (2012) Characterization and quantification of reduced sites on supported vanadium oxide catalysts by using high-frequency electron paramagnetic resonance. ChemCatChem 4:641–652
15. Dinse A, Wolfram T, Carrero C, Schlögl R, Schomäcker R, Dinse KP (2013) Exploring the structure of paramagnetic centers in SBA-15 supported vanadia catalysts with pulsed one- and two-dimensional electron paramagnetic resonance (EPR) and electron nuclear double resonance (ENDOR). J Phys Chem C 117:16921–16932
16. Pöppl A, Manikandan P, Köhler K, Maas P, Strauch P, Böttcher R, Goldfarb D (2001) Elucidation of structure and location of V(IV) ions in heteropolyacid catalysts H4PVMo11O40 as studied by hyperfine sublevel correlation spectroscopy and pulsed electron nuclear double resonance at W- and X-band frequencies. J Am Chem Soc 123:4577–4584
17. Atherton NR (1993) Principles of electron spin resonance. Ellis Horwood Ltd, Hemel, UK
18. Mabbs FE, Collison D (1992) Electron paramagnetic resonance of d-transition metal compounds. Elsevier, Amsterdam, The Netherlands
19. Weil JA, Bolton JR (2007) Electron paramagnetic resonance: elementary theory and practical applications, 2nd edn. Wiley Interscience, New York, USA
20. Brustolon M, Giamello E (eds) (2009) Electron paramagnetic resonance. A practitioner toolkit. Wiley, Hoboken
21. Schweiger A, Jeschke G (2001) Principles of Pulse Electron paramagnetic resonance. Oxford University Press, Oxford, UK
22. Goldfarb D, Stoll S (eds) (2018) EPR spectroscopy. Fundamentals and methods. Wiley Interscience, New York, USA
23. Chiesa M, Livraghi S, Paganini MC, Salvadori E, Giamello E (2020) Nitrogen-doped semiconducting oxides. Implications on photochemical, photocatalytic and electronic properties derived from EPR spectroscopy. Chem Sci 11:6623–6641
24. Brückner A (2003) Monitoring transition metal ions in oxide catalysts during (re)action: the power of operando EPR. Phys Chem Chem Phys 5:4461–4472
25. Brückner A (2010) In situ electron paramagnetic resonance: a unique tool for analysing structure–reactivity relationships in heterogeneous catalysis. Chem Soc Rev 39:4673–4684
26. Zichitella GY, Polyhach Y, Tschaggelar R, Jeschke G, Perez-Ramirez J (2020) Quantification of redox sites during catalytic propane oxychlorination by operando EPR spectroscopy. Angew Chem Int Ed 132:2–9
27. Chiesa M, Giamello E, Livraghi S, Paganini MC, Polliotto V, Salvadori E (2019) Electron magnetic resonance in heterogeneous photocatalysis research. J Phys Condens Matter 31:444001
28. Lunsford JH (1967) EPR study of NO adsorbed on magnesium oxide. J Chem Phys 46:4347–4349
29. Freund H-J, Pacchioni G (2013) Electron transfer at oxide surfaces. The MgO paradigm: from defects to ultrathin films. Chem Rev 113:4035–4072
30. Chiesa M, Che M, Giamello E (2010) EPR characterization and reactivity of surface stabilized inorganic radicals and radical ions. Chem Rev 110:1320–1347
31. Ricci D, Di Valentin C, Pacchioni G, Suskho P, Shluger AL, Giamello E (2003) Paramagnetic defect centers at the MgO surface. An alternative model to oxygen vacancies. J Am Chem Soc 125:738–747
32. Chiesa M, Paganini MC, Giamello E, Di Valentin C, Pacchioni G (2003) First evidence of a single-ion electron trap at the surface of an ionic oxide. Angew Chem Int Ed 42:1759–1761
33. Chiesa M, Paganini MC, Giamello E, Murphy D, Di Valentin C, Pacchioni G (2006) Excess electrons stabilized on ionic oxide surfaces. Acc Chem Res 39:861–867
34. Di Valentin C, Pacchioni G, Chiesa M, Giamello E, Abbot S, Hiez U (2002) NO monomers on MgO powders and thin films. J Phys Chem B 106:1637–1645
35. Martino P, Chiesa M, Paganini MC, Giamello E (2003) Coadsorption of NO and H_2 at the surface of MgO monitored by EPR spectroscopy. Towards a site specific discrimination of polycrystalline oxide surfaces. Surf Sci 527:80–88
36. Paganini MC, Chiesa M, Martino P, Giamello E (2002) EPR study of the surface basicity of calcium oxide. 1. The CaO-NO chemistry. J Phys Chem B 106:12532–12536
37. Chiesa M, Paganini MC, Giamello E, Di Valentin C, Pacchioni G (2003) Bonding of NO on NIxMg1-xO powders: an EPR and computational study. J Mol Catal A 204–205:779–786
38. Che M, Tench AJ (1982) Characterisation and reactivity of mononuclear oxygen species on oxide surfaces. Adv Catal 31:77–133
39. Anpo M, Costentin G, Giamello E, Lauron-Pernot H, Sojka Z (2021) Characterisation and reactivity of oxygen species at the surface of metal oxides. J Catal 393:259–280
40. Giamello E, Ugliengo P, Garrone E (1989) Superoxide ions formed on MgO through the agency of presorbed molecules. Part 1.—Spectroscopic electron spin resonance features. J Chem Soc Faraday Trans I 85:1373–1382
41. Anpo M, Che M, Fubini B, Garrone E, Giamello E, Paganini MC (1999) Generation of superoxide ions at oxide surfaces. Top Catal 8:189–198
42. Garrone E, Giamello E, Ferraris M, Spoto G (1992) Superoxide ions formed on MgO through the agency of presorbed molecules. Part 2.—Details on the mechanism. J Chem Soc Faraday Trans I 88:333–337
43. Brailsford JR, Morton JR, Vannotti LE (1968) Paramagnetic resonance spectra of O- trapped in alkali iodide crystals. J Chem Phys 49:2237–2240
44. Biedrzycki J, Livraghi S, Giamello E, Agnoli S, Granozzi G (2014) Fluorine- and niobium-doped TiO_2: chemical and spectroscopic properties of polycrystalline n-type-doped anatase. J Phys Chem C 118:8462–8473
45. Berger T, Diwald O, Knözinger E, Napoli F, Chiesa M, Giamello E (2007) Hydrogen activation at TiO_2 anatase nanocrystals. Chem Phys 339:138–145
46. Ito T, Lunsford JH (1985) Synthesis of ethylene and ethane by partial oxidation of methane over lithium-doped magnesium oxide. Nature 314:721–722
47. Ito T, Wang JX, Lin LH, Lunsford JH (1985) Oxidative dimerization of methane over a lithium-promoted magnesium oxide catalyst. J Am Chem Soc 107:5062–5068

48. Driscoll DJ, Wilson M, Wang JX, Lunsford JH (1985) Formation of gas-phase methyl radicals over MgO. J Am Chem Soc 35:139–186
49. Nilius N, Levchenko SV, Gonchar A, Risse T, Boatner LA, Frandsen W, Horn R, Freund HJ, Schlögl R, Scheffler M (2010) Temperature-dependent morphology, magnetic and optical properties of Li-doped MgO. ChemCatChem 2:854–862
50. Paganini MC, Chiesa M, Dolci F, Martino P, Giamello E (2006) EPR study of the surface basicity of calcium oxide. 3. Surface reactivity and nonstoichiometry. J Phys Chem B 110:11918–11923
51. Che M, Tench AJ (1983) Characterisation and reactivity of molecular oxygen species on oxide surfaces. Adv Catal 32:1–148
52. Wertz JE, Auzins P, Griffiths JHE, Orton JW (1959) Spin resonance studies of defects in magnesium oxide. Discuss Faraday Soc 28:136–149
53. Murphy DM, Giamello E (1995) A family of trapped electron centers on alkali metal doped magnesium oxide. J Phys Chem 99:15172–15180
54. Chiesa M, Giamello E, Di Valentin C, Pacchioni G, Sojka Z, Van Doorslaer S (2005) Nature of the chemical bond between metal atoms and oxide surfaces: new evidences from spin density studies of K atoms on alkaline Earth oxides. J Am Chem Soc 127:16935–16944
55. Yulikov M, Sterrer M, Heyde M, Rust HP, Risse T, Freund H-J, Pacchioni G, Scagnelli A (2006) Binding of single gold atoms on thin MgO (001) films. Phys Rev Lett 96:146804
56. Baumann S, Paul W, Choi T, Lutz CP, Ardavan A, Heinrich AJ (2015) Electron paramagnetic resonance of individual atoms on a surface. Science 350:417–420
57. Yang K, Willke P, Bae Y, Ferron A, Lado JL, Ardavan A, Fernandez-Rossier J, Heinrich AJ, Lutz CP (2018) Electrically controlled nuclear polarization of individual atoms. Nat Nanotechnol 13:1120–1125
58. Seifert TS, Kovarik S, Juraschek DM, Spaldin NA, Gambardella P, Stepanow S (2020) Sci Adv 6:eabc5511
59. Morra E, Signorile M, Salvadori E, Bordiga S, Giamello E, Chiesa M (2019) Nature and topology of metal-oxygen binding sites in zeolite materials: 17O high resolution EPR spectroscopy of metal loaded ZSM-5. Angew Chem Int Ed 58:12398–12403
60. Oda A, Torigoe H, Itadani A, Ohkubo T, Yumura T, Kobayashi H, Kuroda Y (2013) Success in making Zn+ from atomic Zn0 encapsulated in an MFI-type zeolite with UV light irradiation. J Am Chem Soc 135:18481–18489
61. Li L, Li GD, Yan C, Mu Y, Pan XL, Zou XX, Wang KX, Chen JS (2011) Efficient sunlight-driven dehydrogenative coupling of methane to ethane over a Zn+-modified zeolite. Angew Chem Int Ed 50:8299–8303
62. Iwamoto M, Yahiro H, Tanda K, Mizuno N, Mine Y, Kagawa S (1991) Removal of nitrogen monoxide through a novel catalytic process. 1. Decomposition on excessively copper-ion-exchanged ZSM-5 zeolites. J Phys Chem 95:3727–3730
63. Li Y, Hall WK (1991) Catalytic decomposition of nitric oxide over Cu-zeolites. J Catal 129:202–215
64. Sushkevich VL, van Bokhoven JA (2018) Revisiting copper reduction in zeolites: the impact of autoreduction and sample synthesis procedure. Chem Commun 54:7447–7450
65. Shelef M (1995) Selective catalytic reduction of NOx with N-free reductants. Chem Rev 95:209–225
66. Giamello E, Murphy DM, Magnacca G, Shioya Y, Nomura T, Anpo M (1992) The interaction of NO with copper ions in ZSM5—an EPR and IR investigation. J Catal 136:510–520
67. Sojka Z, Che M, Giamello E (1997) EPR investigation of the electronic structure of mononuclear copper(I) nitric oxide adduct formed upon low-pressure adsorption of NO onto Cu/ZSM-5 zeolite. J Phys Chem B 101:4831–4838
68. Pöppl A, Hartmann M (2002) High-field ESR spectroscopy of Cu(I)-NO complexes in zeolite CuZSM-5. Stud Surf Sci Catal 142A:375–382
69. Umamaheswari V, Hartmann M, Pöppl A (2005) EPR spectroscopy of Cu(I)-NO adsorption complexes formed over Cu-ZSM-5 and Cu-MCM-22 zeolites. J Phys Chem B 109:1537–1546
70. Pietrzik P, Sojka Z (2005) Relativistic density functional calculations of EPR g tensor for η{CuNO}11 species in discrete and zeolite-embedded states. J Phys Chem A 109:10571–10581
71. Pietrzik P, Gil B, Sojka Z (2007) Combining computational and in situ spectroscopies joint with molecular modelling for determination of reaction intermediates of deNOx process—CuZSM-5 catalyst case study. Catal Today 126:103–111
72. Kozyra P, Radon M, Datka J, Broclawik E (2012) On the nature of spin- and orbital-resolved Cu+NO charge transfer in the gas phase and at Cu(I) sites in zeolites. Struct Chem 23:1349–1356
73. Tang J, Zhang T, Ma L, Li L, Zhao J, Zheng L, Lin L (2001) Catal Lett 73:193–197
74. Pietrzyk P, Gora-Marek K, Mazur T, Mozgawa B, Radon M, Chiesa M, Zhao Z, Sojka Z (2021) Structure and mechanistic relevance of Ni^{2+}–NO adduct in model HC SCR reaction over NiZSM-5 catalyst–insights from standard and correlation EPR and IR spectroscopic studies corroborated by molecular modeling. J Catal 394:206–219
75. Wilson ST, Brent ML, Messina C, Cannan TR, Flanigen E (1982) Aluminophosphate molecular sieves: a new class of microporous crystalline inorganic solids. J Am Chem Soc 104:1146–1147
76. Arends LW, Sheldon RA, Wallau M, Schuchardt U (1997) Oxidative transformations of organic compounds mediated by redox molecular sieves. Angew Chem Int Ed 36:1144–2116
77. Chiesa M, Paganini MC, Livraghi S, Giamello E (2013) Charge trapping in TiO_2 polymorphs as seen by electron paramagnetic resonance spectroscopy. Phys Chem Chem Phys 15:9435–9447
78. Maurelli S, Vishnuvarthan M, Chiesa M, Berlier G, Van Doorslaer S (2011) Elucidating the nature and reactivity of Ti ions incorporated in the framework of AlPO-5 molecular sieves. New evidence from 31P HYSCORE spectroscopy. J Am Chem Soc 133:7340–7343
79. Maurelli S, Vishnuvarthan M, Berlier G, Chiesa M (2012) NH_3 and O_2 interaction with tetrahedral Ti^{3+} ions isomorphously substituted in the framework of TiAlPO-5. A combined pulse EPR, pulse ENDOR, UV-Vis and FT-IR study. Phys Chem Chem Phys 14:987–995
80. Maurelli S, Berlier G, Chiesa M, Musso F, Corà F (2014) Structure of the catalytic active sites in vanadium-doped aluminophosphate microporous materials. New evidence from spin density studies. J Phys Chem C 118:19879–19888
81. Leithall R, Shetti V, Maurelli S, Chiesa M, Gianotti E, Raja R (2013) Toward understanding the catalytic synergy in the design of bimetallic molecular sieves for selective aerobic oxidations. J Am Chem Soc 135:2915–2918
82. Schmidt J, Risse T, Hallmann H, Freund H-J (2002) Characterisation of a model Ziegler–Natta catalyst for ethylene polymerisation. J Chem Phys 116:10861–10865
83. Poluboyarov VA, Anufrienko VF, Zakharov VA, Sergeev SA, Makhtarulin SI, Bukatov GD (1984) ESR studies of the state of Ti^{3+} and Ti^{2+} in Ti-Mg catalysts for olefin polymerisation. React Kinet Catal Lett 26:347–351
84. Šindelář P, Matula D, Holeček J (1996) One phase supported titanium based catalyst for polymerisation of ethylene. IV Effect of alkil groups at organoaluminium compound on catalyst performance. J Polym Sci Part A Polym Chem 34:2163–2171
85. Koshevoy EI, Mikenas TB, Zakharov VA, Volodin AM, Kenzhin RM (2014) Formation of isolated titanium(III) ions in superactive

titanium–magnesium catalysts with a low titanium content as active sites in ethylene polymerization. Catal Commun 48:38–40
86. Koshevoy EI, Mikenas TB, Zakharov VA, Shubin AA, Barabanov AA (2016) Electron paramagnetic resonance study of the interaction of surface titanium species with AlR3 cocatalyst in supported Ziegler–Natta catalysts with a low titanium content. J Phys Chem C 120:1121–1129
87. Tregubov AA, Zakharov VA, Mikenas TB (2009) Supported titanium-magnesium catalysts for ethylene polymerization: a comparative study of catalysts containing isolated and clustered titanium ions in different oxidation states. Polym Sci A Polym Chem 47:6362–6372
88. Zakharov VA, Makhtarulin SI, Poluboyarov VA, Anufrienko VF (1984) Study of the state of titanium ions and the composition of the active component in titanium-magnesium catalysts for ethylene polymerization. Makromol Chem 185:1781–1793
89. Morra E, Giamello E, Van Doorslaer S, Antinucci G, D'Amore M, Busico V, Chiesa M (2015) Probing the coordinative unsaturation and local environment of Ti^{3+} sites in an activated high-yield Ziegler–Natta catalyst. Angew Chem Int Ed 54:4857–4860
90. Allouche F, Klose D, Gordon CP, Ashuiev A, Wörle M, Kalendra V, Mougel V, Copéret C, Jeschke G (2018) Low-coordinated titanium (III) alkyl—molecular and surface—complexes: detailed structure from advanced EPR spectroscopy. Angew Chem Int Ed 57:14533
91. Ashuiev A, Allouche F, Willi N, Searles K, Klose D, Copéret C, Jeschke G (2021) Molecular and supported Ti(III)-alkyls: efficient ethylene polymerization driven by the π-character of metal–carbon bonds and back donation from a singly occupied molecular orbital. Chem Sci 12:780–792
92. Salvadori E, Chiesa M, Buonerba A, Grassi A (2020) Structure and dynamics of catalytically competent but labile paramagnetic metal-hydrides: the Ti(III)-H in homogeneous olefin polymerization. Chem Sci 11:12436–12445
93. Podvorica L, Salvadori E, Piemontesi F, Vitale G, Morini G, Chiesa M (2020) Isolated Ti(III) species on the surface of a preactive Ziegler Natta catalyst. Appl Magn Reson 51:1515–1528
94. Chiesa M, Giamello E, Di Valentin C, Pacchioni G (2005) The 17O hyperfine structure of trapped holes photo generated at the surface of polycrystalline MgO. Chem Phys Lett 403:124–128
95. Livraghi S, Maurelli S, Paganini MC, Chiesa M, Giamello E (2011) Probing the local environment of Ti^{3+} ions in TiO_2 (rutile) by 17O HYSCORE. Angew Chem Int Ed 50:8038–8040
96. Lagostina V, Salvadori E, Chiesa M, Giamello E (2020) Electron paramagnetic resonance study of vanadium exchanged H-ZSM5 prepared by vapor reaction of VCl4. The role of 17O isotope labelling in the characterisation of the metal oxide interaction. J Catal 391:397–403
97. Kaupp M, Bul M, Malkin VG (eds) (2004) Calculation of NMR and EPR parameters, theory and applications. Wiley Interscience, New York, USA